

A Young Super Star Cluster Powering a Nebula of Retained Massive Star Ejecta

MASSIMO PASCALE¹ AND LIANG DAI²

¹*Department of Astronomy, University of California, 501 Campbell Hall #3411, Berkeley, CA 94720, USA*

²*Department of Physics, University of California, 366 Physics North MC 7300, Berkeley, CA. 94720, USA*

ABSTRACT

We suggest that “Godzilla” of the lensed Sunburst galaxy ($z = 2.37$) is a young super star cluster powering a nebula of gravitationally trapped stellar ejecta. Employing HST photometry and spectroscopy from VLT/MUSE and VLT/X-Shooter, we infer physical and chemical properties of the cluster and nebula, finding Godzilla is young (4–6 Myr), massive ($\sim 10^{6-7} M_{\odot}$), a stellar metallicity $Z \simeq 0.25 Z_{\odot}$, and has a compact FUV component (\lesssim few parsecs). The gas is significantly enriched with N and He, indicating stellar wind material, and has highly elevated O relative to the stellar metallicity, indicating entrainment of CCSNe ejecta. The high density $n_e \simeq 10^{7-8} \text{ cm}^{-3}$ implies a highly pressurized intracluster environment. We propose the pressure results from CCSN-driven supersonic turbulence in warm, self-shielding gas, which has accumulated in the cluster center after runaway radiative cooling and is dense enough to resist removal by CCSNe. The nebula gas shows sub-solar C/O, Ne/O and Si/O, which may reflect the CCSN element yields for initial stellar masses $> 40 M_{\odot}$. A comparison to element yield synthesis models for young star clusters shows the gas abundances are consistent with complete retention and mixture of stellar winds and CCSNe ejecta until the inferred cluster age. The inferred O and He enhancement may have implications for the formation of multiple stellar populations in globular clusters, as stars formed from this gas would contradict the observed abundances of second-population stars.

1. INTRODUCTION

The Sunburst Arc, a Cosmic Noon Lyman- α emitter at $z_s = 2.37$ (Dahle et al. 2016) in the lensing field of the galaxy cluster PSZ1 G311.65-18.48 at $z_l = 0.443$ (Planck Collaboration et al. 2014), is a spectacular gravitationally magnified galaxy (Rivera-Thorsen et al. 2017, 2019). With spectroscopic confirmation, the arc hosts an apparently unresolved source bright in rest-frame FUV ($m_{F814W} \approx 22$; Figure 1), which has been given the nickname “Godzilla” (Diego et al. 2022).

Godzilla exhibits several enigmatic aspects. Much to the surprise of lens modellers, it has no confirmed counter lensed images elsewhere on the arc with comparable magnitudes, despite that multiple lens models predict so (Vanzella et al. 2020a; Pignataro et al. 2021; Diego et al. 2022; Sharon et al. 2022). This implies a compact source size, with a flux enhanced by invisible milli-lenses such as sub-galactic dark matter halos (Dai et al. 2020; Diego et al. 2022, 2023). Moreover, Godzilla shows a highly unusual nebular spectrum from rest-frame FUV to optical. Vanzella et al. (2020b) first inferred extremely high electron density for the ionized gas $n_e \gtrsim 10^6 \text{ cm}^{-3}$ from CIII] $\lambda\lambda$ 1908, 1906 and SiIII] $\lambda\lambda$ 1892, 1883 line ratios, and commented on the

striking weakness of hydrogen Balmer lines (Vanzella et al. 2020b). Vanzella et al. (2020b) also detected rare Bowen fluorescence of Fe III lines pumped by Ly α radiation, implying an optically thick gaseous environment that efficiently traps but does not destroy Ly α photons.

Diego et al. (2022) considered multiple possibilities for the underlying nature of Godzilla, which include a bright stellar transient such as an ongoing luminous blue variable magnified by $\sim 10^4$ fold, a hyper-luminous supermassive star, or a luminous accretion disk around an intermediate mass black hole. Stringent limits on continuum photometric variability over the timescale of ~ 2 yr in the source frame constrain the transient scenario. On the other hand, no detailed spectral models have been presented thus far to substantiate the above hypotheses. In this paper, we suggest that Godzilla is likely a compact young massive star cluster powering nebular emission, which we deem more probable as Sunburst is found to be vigorously forming stars in clusters (Vanzella et al. 2022). Compared to the Lyman-continuum-leaking (LyC) star cluster in the same galaxy which has been extensively studied (Chisholm et al. 2019; Vanzella et al. 2022; Mainali et al. 2022; Pascale et al. 2023; Kim et al. 2023; Mestric et al. 2023; Rivera-Thorsen et al. 2024), Godzilla shows a similar shape of

the FUV continuum as well as prominent stellar wind features tracing O stars (e.g. C IV λ 1550 P Cygni profile; Figure 3), lending support to the star cluster interpretation. Narrow (FWHM $\lesssim 100 \text{ km s}^{-1}$) emission lines of various metal ions (O II, O III, N III, C III, Ne III, Si III) are consistent with photoionization by O stars within a star-cluster-scale gravitational potential, but ions requiring more energetic ionizing sources such as an AGN are unseen. If our model is correct, detailed study of Godzilla will greatly deepen our understanding of feedback and self-enrichment from clustered star formation in dense environments at the culmination of cosmic star formation.

In this work, we perform a joint photometric and spectroscopic analysis using archival Hubble Space Telescope (HST) imaging and ground-based Very Large Telescope (VLT) MUSE and VLT/X-shooter spectroscopy. To infer the physical parameters of the system and the chemical abundances of the nebular gas, we follow a methodology which was successfully applied to the LyC cluster of the same galaxy in Pascale et al. (2023) (hereafter P23), fitting a spectral energy distribution (SED) to match broad-filter photometry and nebular emission line fluxes. Informed by this inference, we then construct a self-consistent physical model supported by the data.

Our modeling suggests that the cluster has an age $\sim 4\text{--}6$ Myr and has a stellar metallicity similar to the Small Magellanic Cloud (SMC), consistent with the expectations from observed stellar wind features (Chisholm et al. 2019). Electron density diagnostics including the CIII] λ 1908, 1906 and SiIII] λ 1892, 1883 line ratios and the relative strengths between [O III] λ 4959, 5007 and [O III] λ 1660, 1666 confirm an unusually high density $n_e \sim 10^{(7-8)} \text{ cm}^{-3}$, corresponding to a pressure on the order $\log P [\text{K cm}^{-3}] \sim 11\text{--}12$. Exciting such dense gas requires an enormous hydrogen ionizing photon flux $\log \Phi(\text{H}^0) [\text{s}^{-1} \text{ cm}^{-2}] \sim 15\text{--}16$, which constrains the nebula to be smaller than ~ 1 pc and likely places it within the cluster. Remarkably, we find evidence of gas-phase abundance enhancement in N, C, O, and He, such that the nebula gas exhibits solar-like O/H, high N/O similar to high- z N-emitters (Marques-Chaves et al. 2024), yet sub-solar C/O, Si/O and Ne/O. We suggest this is due to self-enrichment by massive star winds and core-collapse supernova (CCSN) ejecta, and corroborate this hypothesis through a comparison with synthetic light element yield models.

These remarkable properties may be a natural consequence of young star cluster evolution in the regime of high mass and high compactness. We develop a physical picture where the ejecta of winds and CCSNe stays inside the cluster through rapid radiative cooling (Wünsch

et al. 2011, 2017a), but is dynamically supported by supersonic turbulence driven by CCSNe. This physical picture, depicted in Figure 2, congruently interprets the unusual dataset; it can simultaneously explain the observed high electron density, high pressure, ionization parameter, and chemical abundances indicative of retention of stellar ejecta, and may provide the required gas geometry for Ly α -pumped Fe fluorescence.

The remainder of this paper will be organized as the following. In Section 2, we summarize the public imaging and spectroscopic datasets used in this work. In Section 3 and Section 4, we discuss how we will model broad-band photometry and emission lines for the star cluster and its nebula by applying BPASS stellar population synthesis models and Cloudy photoionization calculations. In particular, we will discuss how we extend our Cloudy calculations to allow for non-standard gas-phase element abundances. In Section 5, we present results for joint photometric and emission line fitting for two models and infer key physical and chemical properties of the star cluster and its ionized gas. In Section 6, we discuss the implications of our fitting results for the dynamics, chemical composition, and astrophysical origin of Godzilla’s nebula. Concluding remarks will be provided in Section 7.

2. DATA

In this section, we summarize the archival data used in this work: HST imaging data, VLT/MUSE IFU spectroscopy, and VLT/X-shooter slit spectroscopy.

2.1. HST Imaging

Observations for PSZ1 G311.65-18.48 were obtained across multiple programs between 2018 and 2020 (P.I. Dahle Program ID 15101, P.I. Gladlers Program ID 15949, P.I. Bayliss Program ID 15377). In this work, we make use of observations publicly available on the MAST archive for 15 filters: WFC3/UVIS F390W, WFC3/UVIS F410M, WFC3/UVIS F555W, WFC3/UVIS F606W, ACS/WFC F814W, WFC3/UVIS F098M, WFC3/IR F105W, WFC3/IR F125W, WFC3/IR F126N, WFC3/IR F128N, WFC3/IR F140W, WFC3/IR F153M, WFC3/IR F160W, WFC3/IR F164N, WFC3/F167N. All UVIS+WFC images were aligned to a common pixel scale of 30 mas/pixel, while all IR images were aligned to a pixel scale of 60 mas/pixel using the astropy `reproject` package in combination with `astroalign` (Beroiz et al. 2020).

2.2. VLT/MUSE IFU Spectroscopy

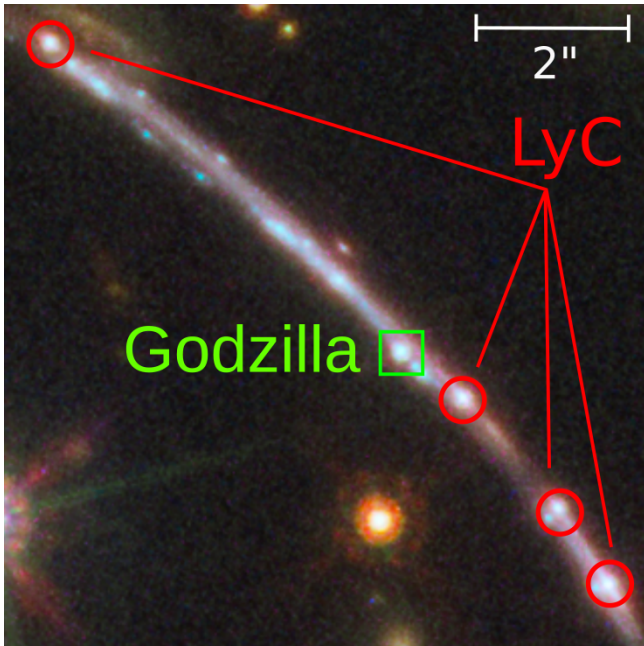


Figure 1. *HST* false color image of the Sunburst Arc with the lone image of Godzilla and four images of the Lyman-continuum-leaking (LyC) cluster marked. Godzilla appears similarly bright to the multiple images of the LyC cluster, so naively multiple counter-images of Godzilla would be detectable in a typical strong-lensing configuration. However, the non-detection of counter-images and time variability favors the hypothesis that Godzilla is milli-lensed and highly magnified.

We use reduced MUSE IFU science datacubes publicly accessible from the ESO archive¹. Two datacubes are used, which cover the observed wavelength range 475–935 nm at $R \approx 2600$ –3000 and were calibrated and reduced with the standard reduction pipeline: one obtained on May 13 and Aug 24 in 2016 (Program 107.22SK; PI: E. Vanzella; total exposure 4449 s), and another on Aug 10, 2021 (Program 297.A-5012; PI: N. Aghanim; total exposure 2808 s). The MUSE IFU observations were carried out in the Wide Field Mode under a typical seeing condition $\text{FWHM} = 0.5$ – $0.6''$, achieving a spatial resolution 1.4– $2''$ on the sky. Through a comparison between the two datacubes, we do not find any evidence for spectral variability, so we properly combine them to achieve the best signal-to-noise ratio for emission lines.

2.3. VLT/X-shooter Slit Spectroscopy

X-shooter slit spectroscopy data reduced with the standard reduction pipeline are accessed from the ESO archive. Data were collected from Program 0103.A-

Table 1. Inferred isotropic luminosities for nebular emission lines detected from VLT/MUSE IFU data for Godzilla. The isotropic luminosity is calculated for a luminosity distance of $d = 19.566$ Gpc (corresponding to the source redshift $z_s = 2.369$) and a fiducial achromatic magnification factor $\mu = 300$, and is uncorrected for dust reddening.

Emission line	Luminosity L [10^{38} erg s $^{-1}$]
O I λ 1641	26 ± 4
[O III] λ 1660	21 ± 7
[O III] λ 1666	55 ± 6
N III] λ 1750	73 ± 12
N III] λ 1752	29 ± 5
[Si III] λ 1883	$\lesssim 8$
Si III] λ 1892	54 ± 4
[C III] λ 1906	$\lesssim 10$
C III] λ 1908	123 ± 8
[O II] λ 2471	14 ± 4

Table 2. Inferred isotropic luminosities of nebular emission lines detected from VLT/X-shooter for Godzilla. The same luminosity distance and fiducial magnification factor $\mu = 300$ are used as in Table 1, while dust reddening is not corrected for. We have applied a wavelength independent PSF correction factor = 1.2 using a theoretical Moffat PSF model with $\beta = 4.765$.

Emission line	Luminosity L [10^{38} erg s $^{-1}$]
Ly α	$\lesssim 240$
[O II] λ 3726	$\lesssim 42$
[O II] λ 3729	$\lesssim 24$
[Ne III] λ 3869	37 ± 7
[Ne III] λ 3967	$\lesssim 12$
H β	$\lesssim 61$
[O III] λ 4959	$\lesssim 61$
[O III] λ 5007	$\lesssim 180$
H α	$\lesssim 185$
He I λ 5879	36 ± 18

0688 (PI: E. Vanzella). Exposures were obtained under typical seeing conditions $\text{FWHM} \sim 0.5$ – $0.6''$. Slit spectra covering observed 994–2479 nm ($R \approx 8000$) are used for extracting fluxes for rest-frame NUV and optical emission lines, while additional spectra covering observed 534–1020 nm ($R \approx 11000$) are used for cross-checking strong FUV emission lines. For accessing spatially resolved spectral information, we carry out flux calibration of the 2D spectra by comparing the flux-calibrated and flux-uncalibrated 1D spectra, and then extract fluxes at the location of Godzilla.

3. PHOTOMETRY

¹ <http://archive.eso.org/scienceportal/home>

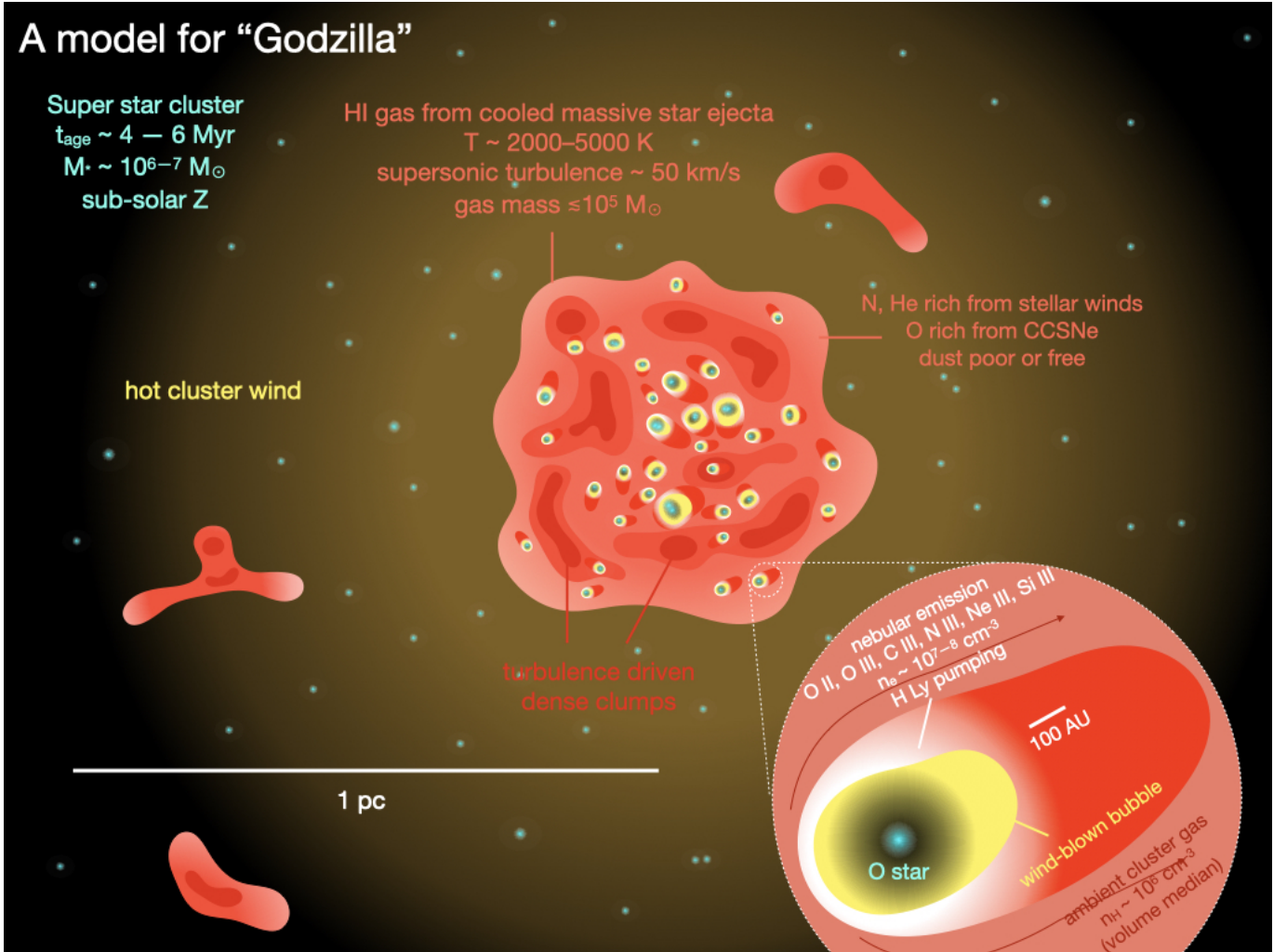


Figure 2. Illustration of our favored physical model for Godzilla and its nebula. Due to highly efficient radiative cooling, massive star ejecta from winds and CCSNe has accumulated at the center of a massive, compact young star cluster, forming self-shielded neutral warm gas in a state of supersonic turbulence driven by energy injection from CCSNe. Situated in an extreme radiation environment, this gravitationally retained gas likely has little to no dust. As a result, it is optically thick to ionizing photons but is transparent to UV and optical photons. O stars embedded inside it drive individual wind-blown hot bubbles in which the observed nebula emission lines are excited.

Following the methods of P23, we measure the PSF of each HST image using the `photutils` package by stacking isolated, unsaturated stars in the field. An initial catalog of stars is generated using `DAOSTARFinder` following Stetson (1987), and then each star is vetted by eye to be isolated and unsaturated, resulting in a final catalog of dozens of stars. The final star list is extracted into centered cutouts which are normalized and median-subtracted to mitigate sky background, and the cutouts are stacked into an oversampled PSF using the `EPSFBuilder` function.

To measure fluxes for Godzilla, we model the surface brightness profile as a Sérsic profile convolved with the PSF (Sersic 1968). There are two primary sources of contamination which complicate fitting: neighboring

star-formation knots on the arc and the diffuse arc background itself. Each of the neighboring knots are observed to be consistent with PSF profiles and are simultaneously fit in PSF photometry. The arc background is modeled as a thick line of smoothly-varying surface brightness, with free parameters for slope, intercept, and normalization. This simple parametrization is found to well approximate the arc background locally (within $\sim 1 - 2''$), and is fit simultaneously to Godzilla and neighboring knots. As an example, the best fit model and residual for the F814W filter is shown in Figure 4.

Across all HST images, the best-fit Sérsic profiles for Godzilla consistently have $r_{\text{eff}} \lesssim 1$ pixel, implying that Godzilla is unresolved or at most marginally-resolved. This constrains the spatial extent $R_{\text{FUV}} \lesssim 4$ pc ($150/\mu_t$)

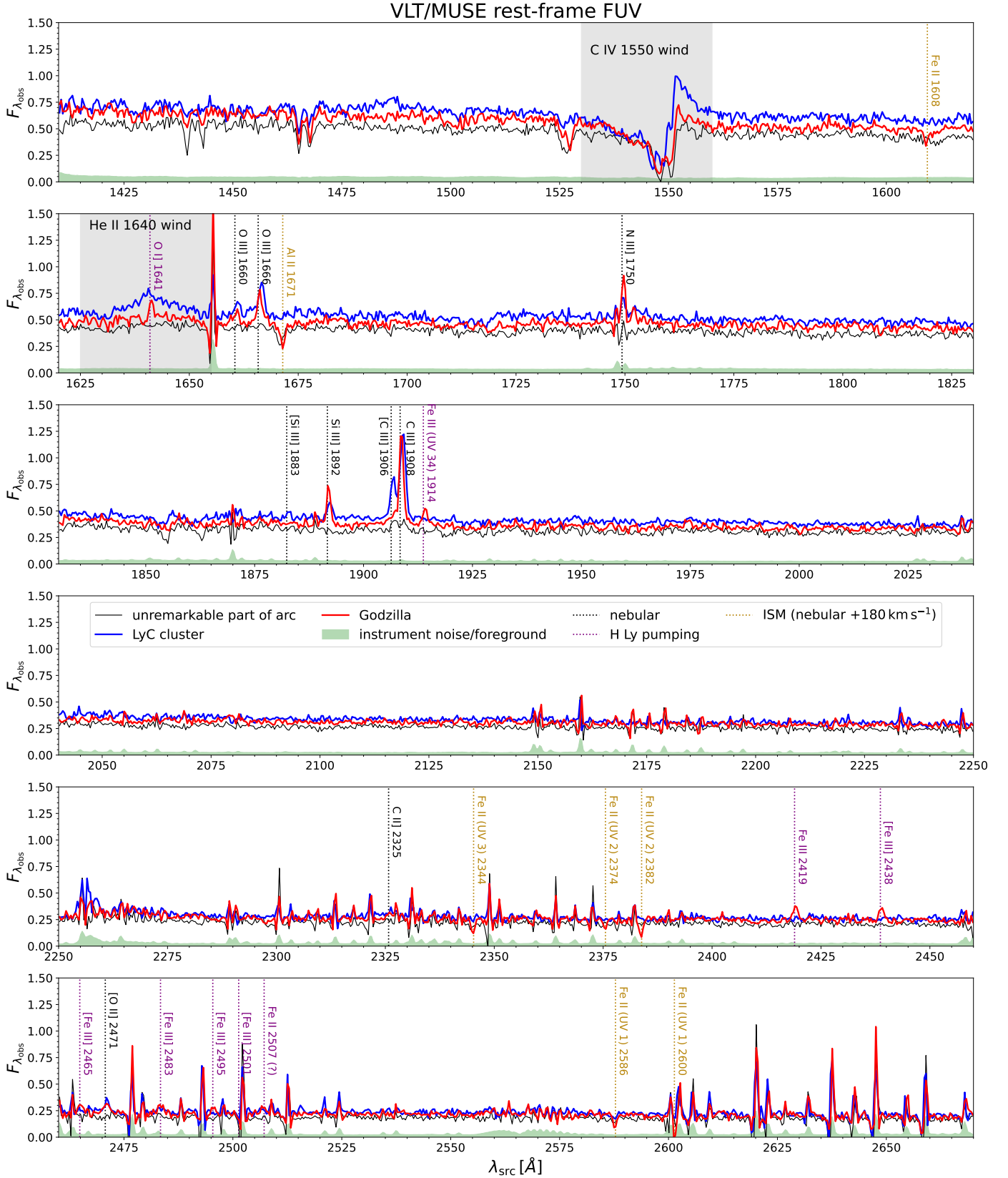


Figure 3. MUSE IFU spectrum in the rest-frame wavelength range 1410–2670 Å (observed flux density $F_{\lambda_{\text{obs}}}$ in units of 10^{-17} erg s⁻¹ cm⁻² Å⁻¹). We compare specific fluxes extracted from three circular apertures of radius 0.5'', centered on *Godzilla* (red), the LyC leaking star cluster (Vanzella et al. 2020a) (blue), as well as another unremarkable region on the Sunburst Arc (black), respectively. We mark narrow nebular emission lines (black dotted), ISM absorption lines (dotted yellow), and additional unusual emission lines related to H Lyman pumping (dotted magenta).

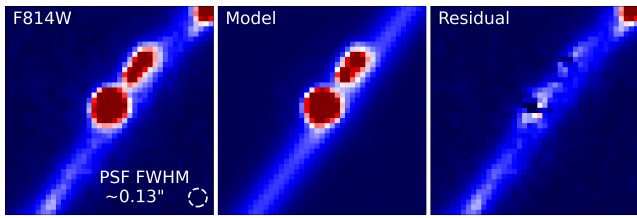


Figure 4. Example of surface brightness modeling of Godzilla and the host arc in F814W. Godzilla is modeled as a Sérsic profile convolved with the PSF, and its neighboring knots are modeled as simple PSFs. The underlying arc background is approximated as a line convolved with a 2D-Gaussian, for which the line slope and intercept, as well as the Gaussian width are free parameters. We find that, even in the highest resolution filters, the best fit Sérsic for Godzilla has effective radius $r_{\text{eff}} < 1$ pixel, consistent with an unresolved FUV source. For a fiducial tangential magnification value $\mu_t = 150$, this implies a physical size for the OB star component $R_{\text{FUV}} < 4$ pc.

Table 3. HST photometry for Godzilla. Lensing magnification is uncorrected for.

Filter	AB magnitude	Spectral features
F275W ^a	$\gtrsim 28.6$	Rest-frame LyC;
F390W ^a	22.41 ± 0.10	Ly α & damping wing
F410M ^a	22.88 ± 0.10	Ly α & damping wing
F555W	22.00 ± 0.05	–
F606W	22.00 ± 0.05	–
F814W	22.00 ± 0.05	–
F098M	22.18 ± 0.10	–
F105W	22.16 ± 0.10	–
F125W	22.18 ± 0.10	–
F126N	22.16 ± 0.10	[O II] $\lambda\lambda 3727, 3729$
F128N	22.24 ± 0.15	–
F140W	22.18 ± 0.10	–
F153M	22.28 ± 0.10	–
F160W	22.17 ± 0.10	H β , [O III] $\lambda\lambda 4959, 5007$
F164N ^a	22.17 ± 0.10	H β
F167N	22.05 ± 0.10	[O III] $\lambda 4959$

^aExcluded from analysis.

of the OB star population, for a given tangential magnification μ_t . The statistical errors from fitting are likely subdominant to systematics involving parametrization of the various components – to account for this we set a conservative photometric error of 0.05 mag for the WFC3/UVIS and ACS/WFC filters and 0.1 mag for the WFC3/IR filters.

4. SPECTRAL MODELING

To unveil the nature of Godzilla and the origin of its nebular emission, we study several physical models describing a young mass star cluster associated with a photoionization nebula. We will adopt an iterative strategy. We shall first study simple models; if significant discrepancy with data is identified, we will be guided to consider models describing more unusual but physically motivated situations.

To that end, we will perform joint photometric-spectroscopic fitting using photometry from 12 HST filters (Table 3) and 18 emission line flux detections or upper limits from VLT/MUSE and VLT/X-shooter (Table 1 and Table 2). We shall include only 12 of the 15 available HST filters in fitting. Photometry in F390W and F410M are sensitive to Ly α line transfer and damping wing effects, which we do not attempt to carefully model. We also exclude F164N; while this filter constrains H β , we are aware of a flux calibration issue in this filter (Kim et al. 2023).

While several filters cover emission lines including [OII] $\lambda\lambda 3726, 3729$ (F126N), H β (F160W, F164N), and [OIII] $\lambda\lambda 4959, 5007$ (F160W), they appear weak and only flux upper limits are reliable. We note that HST photometry is significantly more sensitive and hence may constrain these emission lines better than X-shooter data.

Emission line measurements prove highly valuable in probing the properties of Godzilla’s nebula gas. Even many upper limits are surprisingly informative. The C III] $\lambda\lambda 1908, 1906$ and Si III] $\lambda\lambda 1892, 1883$ line ratios probe the electron density in a high ionization environment. Non-detection of the forbidden component (Vanzella et al. 2020b) indicates that Godzilla has a nebula much denser than what are often considered dense high- z HII regions with $3 \lesssim \log n_e [\text{cm}^{-3}] \lesssim 6$ (Keenan et al. 1992; Jaskot & Ravindranath 2016). Ratios between the O II and O III lines [OII] $\lambda 2471$ /[OIII] $\lambda\lambda 1660, 1666$ (Kewley et al. 2019) are sensitive to ionization degree and electron temperature (Kewley & Dopita 2002; Kobulnicky & Kewley 2004; Dors et al. 2011). For Godzilla, the [OIII] $\lambda\lambda 1660, 1666$ /[OIII] $\lambda\lambda 4959, 5007$ line ratios also constrain the electron density, as these trace the same ion but the rest-frame optical doublet has a much lower critical density at $6.4 \times 10^5 \text{ cm}^{-3}$ (Draine 2011a).

4.1. Base Model

We first study a model describing photoionized gas excited by the entire star cluster. This has been used to model the spectrum of the Lyman-continuum-leaking cluster of the Sunburst Arc in P23. The model star cluster SED is taken from BPASS (v2.0) with binary stellar evolution accounted for (Stanway et al. 2016).

For a compact, massive star cluster, we consider an instantaneous burst of star formation with an initial mass function (IMF) $\xi(m) \propto m^{-1.3}$ for $m < 0.5 M_{\odot}$ and $\xi(m) \propto m^{-2.35}$ for $m > 0.5 M_{\odot}$ in the initial stellar mass range $0.1 < m/M_{\odot} < 300$. The cluster is characterized by the age t_{age} and stellar metallicity Z as free parameters.

Following the method of P23, nebular continuum, emission lines, and attenuation of incident star light are all modeled with the `Cloudy` code (v17 Ferland et al. 2017) assuming a plane-parallel, stratified structure locally. The nebula gas is assumed to be isobaric, such that it is characterized by the typical dimensionless ionization parameter U and the constant pressure P . In Bayesian inference, we shall use log-flat priors for these, in the range $-3 \leq \log U \leq -1$ and $6 \leq \log P [\text{K cm}^{-3}] \leq 13$.

When running `Cloudy` calculations for the Base Model, we identify the stellar metallicity Z with the gas-phase metallicity and use a rescaled solar abundance pattern (see Table 7.1 or the `Cloudy` manual HAZY 1), with non-rescaled-solar prescriptions for He (following Russell & Dopita 1992), C, and N (following Dopita et al. 2006). The abundances of N, C, Ne, and Si are allowed to freely vary only when we fit the emission line data; we do this by rescaling the fluxes of emission lines corresponding to these elements. This is a computationally efficient and justifiable approximation provided that varying the abundance of these elements does not significantly change line cooling.

We also introduce two geometric parameters: the parameter x ($0 \leq x \leq 1$) is the fraction of ionizing radiation processed by the nebular gas. A second parameter, y , describes the fraction of nebular gas toward which our sight-line is intervened by HI gas ($y = 0$) versus the fraction toward which the sight-line is not ($y = 1$). We shall refer to the former case as “HI-obscured” (see Figure 2 of P23). For example, the latter case can correspond to directly seeing the irradiated side of the HII zone on the surface of a self-shielding cloud, without any intervening gas. The former case can correspond to viewing from the back side of the self-shielding cloud, so that photons reaching the observer must pass through a substantial HI column of the cloud. Without internal dust attenuation, the parameter y does not affect (semi-)forbidden lines, but has an impact on lines with a significant optical depth effect or with a large diffusive contribution in the HI layer.

P23 introduced a third geometric parameter, z , which measures the fraction of star light along the line-of-sight that is obscured by photoionized gas. Running `Cloudy` models without internal dust, we do not find it strongly

constrained by data and hence set it to zero obscuration. Finally, we also incorporate external dust reddening, fixing Milky Way extinction following the galactic dust maps of Schlegel et al. (1998), and fitting for host galaxy ISM dust reddening following the law of Reddy et al. (2015), where the normalization $E(B-V)$ is left free. In total, the Base Model has 10 free parameters.

4.2. Chemically Anomalous Model

In Godzilla, some unusual emission line ratios hint at the possibility of non-standard gas-phase element abundances. Apart from a clear detection of N enhancement (like what we found for the LyC cluster in P23), we see evidence for He and O enhancement, as well as unusual C/O and Ne/O ratios. The surprising weakness of H Balmer lines relative to metal forbidden lines (Vanzella et al. 2020b) may also be related to an unusual abundance pattern.

Chemical self-enrichment is physically plausible for newborn massive star clusters if massive star ejecta can be retained in the cluster vicinity or interior (de Mink et al. 2009; Martell et al. 2013; Lochhaas & Thompson 2017a). Massive star winds or envelope stripping may cause self-enrichment of N and He, while CCSNe produce α -elements including O, Ne and Si. We are therefore motivated to consider more sophisticated non-rescaled-solar abundance patterns. In particular, the gas-phase oxygen abundance may be enhanced compared to the interior of stars. Unlike N, C, Si, and Ne, oxygen ions play a significant role in line cooling, and hence changes in oxygen abundance cannot be simply accounted for by rescaling O line fluxes in post-processing.

In the Chemically Anomalous Model, the stellar SED is the same as in the Base Model. We fix the stellar and gas-phase (before self-enrichment) metallicities to $0.25 Z_{\odot}$ following the best-fit Base Model. This gas-phase metallicity is consistent with what we found for the LyC cluster of Sunburst in P23, and within the inference uncertainty agrees with the gas metallicity determined by Rivera-Thorsen et al. (2024). We then compute a grid of `Cloudy` models for which O/H varies from one-fourth to twice the solar value (assuming $12 + \log(\text{O}/\text{H})_{\odot} = 8.69$) (Asplund et al. 2021). Similarly, He abundance variation should be consistently treated with `Cloudy`. The detection of the recombination line He I λ 5879 probes He/H, which may be enhanced by evolved star winds. We create a He/H grid to allow enhancement up to five times greater than the prescription of Russell & Dopita (1992) at one-fourth solar metallicity. In this model, the stellar metallicity is no longer a free parameter in fitting, while gas-phase O and He abundances are

now left free to vary, increasing the total number of free parameters to 11.

5. RESULTS

We fit the two models to data from 12 filters of HST photometry (Fig. 5) and 18 emission line fluxes and upper limits (Fig. 6). We use the sampler `PyMultinest` (Feroz et al. 2009; Buchner et al. 2014) with 1,000 live points running for 10,000 steps to explore the model parameter space and derive posterior samples. Below we discuss the inferred physical parameters and the fitting performance for each model. We assign uncertainties in both filter photometry and emission line fluxes/upper limits conservatively, and hence the reduced chi-squared $\chi^2_\nu < 1$ obtained in our fitting is likely indicative of overestimated errorbars rather than overfitting.

5.1. Base Model

The Base Model well-reproduces all observables with a reduced chi-squared $\chi^2_\nu = 0.52$. However, constraints on the stellar properties are not extremely stringent. Using the BPASS instantaneous burst model, photometry of the stellar and nebular continuum indicates a high stellar mass $\log \mu M_\star/M_\odot = 9.29^{+0.11}_{-0.16}$, or $M_\star/M_\odot = 6 \times 10^6 (300/\mu)$. The magnification of Godzilla is not known as multiple lens models make a range of predictions (Pignataro et al. 2021; Diego et al. 2022; Sharon et al. 2022). The surprising absence of bright counter images imply that Godzilla’s magnification factor may have been strongly boosted by milli-lensing (Diego et al. 2022). Hereafter, we shall use a high fiducial value $\mu = 300$ and denote $\mu_{300} = \mu/300$.

The favored cluster age is in the range $t_{\text{age}} = 3\text{--}6$ Myr. Godzilla thus appears more evolved than the LyC cluster. As seen in Fig. 3, the emission component of the C IV λ 1550 P Cygni wind feature, whose strength is sensitive to age but not stellar metallicity (Leitherer et al. 2014; Chisholm et al. 2019), has a significantly lower equivalent width than for the LyC cluster in the same galaxy ($t_{\text{age}} \sim 3$ Myr; Chisholm et al. 2019; Pascale et al. 2023). The higher cluster age is further corroborated by the absence of broad He II λ 1640 emission, a unique signature of Very Massive Stars ($> 100 M_\odot$) seen in the LyC cluster that would likely have died by $t_{\text{age}} = 3\text{--}4$ Myr (Mestric et al. 2023).

The stellar and gas metallicity is constrained to be $\log Z = -2.29^{+0.16}_{-0.12}$, or 20%–40% of the solar value. The broad posterior distribution for Z is likely due to non-detections of H α , H β , and the [O III] $\lambda\lambda$ 4959,5007 doublet. Reassuringly, the median of the posterior matches the value inferred for the LyC cluster in P23 and Rivera-Thorsen et al. (2024), as the two objects reside in the

same galaxy. For a further piece of evidence, we use the depth of the absorption component of the C IV λ 1550 P Cygni wind feature, which is primarily set by the stellar metallicity (Chisholm et al. 2019). The depths are observed to be consistent in both Godzilla and the LyC cluster (Fig. 3). Similar to Kim et al. (2023), we find a minimal amount of external dust reddening $E(B - V) = 0.02^{+0.02}_{-0.02}$ based on the continuum shape.

Remarkably, the ionized gas of Godzilla has an extremely high pressure $\log P = 11.56^{+0.14}_{-0.12}$ [K cm $^{-3}$] and a low ionization parameter $\log U = -2.61^{+0.13}_{-0.11}$, corresponding to a characteristic incident ionizing flux $\log \Phi(\text{H}^0) = 15.22^{+0.16}_{-0.15}$ [s $^{-1}$ cm $^{-2}$] and a high electron density $\log n_e = 7.12^{+0.30}_{-0.15}$ [cm $^{-3}$].

The Base Model allows the abundances of C, N, Ne and Si to vary freely in emission line fitting. We find all four to show unusual abundances relative to oxygen, with lower C/O, Ne/O and Si/O but significantly higher N/O compared to typical ISM values found in galaxies at sub-solar metallicity. The elevated N/O, $\log(\text{N}/\text{O}) = -0.30^{+0.07}_{-0.07}$, is reminiscent of the LyC cluster, a factor of ~ 13 greater than typical HII region abundances (Pilyugin et al. 2012). Thus, Godzilla appears to be another example of nitrogen emitters which have received heated discussion in the literature (Marques-Chaves et al. 2024).

While the measured $\log \text{C}/\text{O} = -0.79^{+0.05}_{-0.05}$ is low compared to the solar value of -0.30 (Asplund et al. 2021), we note that it is consistent with the ~ -0.7 ISM value observed in $z \sim 2\text{--}3$ galaxies at a similar metallicity (Berg et al. 2019) (see § 6.3). The gas-phase Si/O appears low, $\log(\text{Si}/\text{O}) = -1.84^{+0.06}_{-0.05}$, a factor of 4–5 lower than the solar value -1.15 (Asplund et al. 2021). While grain depletion of Si may explain this, it may also point towards the intriguing possibility of self-enrichment of oxygen by CCSNe that go off in the star cluster. This, taken with the low C/O and the anomalously low measured $\log(\text{Ne}/\text{O}) = -1.20^{+0.11}_{-0.12}$ (factor of ~ 5 deficient relative to the solar value) motivates us to consider more sophisticated gas abundance models in which the gas-phase oxygen abundance differs from the stellar value.

The parameter y is tightly constrained to be very close to zero, $y < 0.03$, which implies that nearly all the nebular emission that we see is HI-obscured, mostly likely by the HI gas right behind the edge of the HII zone in an ionization-bounded geometry. The strong preference for this in data is driven by the need to significantly decrease the H Balmer lines. In Section 6.6, we discuss how H Balmer lines might be reduced by a dust-free HI zone.

5.2. Chemically Anomalous Model

To explore self-enrichment of gas-phase abundances, we fix the stellar metallicity to be $Z = 0.25 Z_{\odot}$ in the Chemically Anomalous Model, which corresponds approximately to the median of the posterior distribution of the Base Model as well as the Z value inferred for the LyC cluster in P23. In constructing `CLOUDY` model grids, we scan a range of O/H and He/H values. The goodness of fit is notably improved over the Base Model, achieving a lower $\chi_r^2 = 0.39$ despite only one more free parameter. For this reason, we think that the best-fit Chemically Anomalous Model reflects reality more than the best-fit Base Model.

For most parameters, we find posterior distributions consistent with what we derive for the Base Model (Table 4). There are three notable exceptions: (1) a lower value for the effective area covering factor $x \simeq 0.2$ is now preferred; (2) the gas pressure is ~ 0.3 dex higher at $\log P \sim 11.9$; (3) the posterior distribution of the ionization parameter keeps a peak at low values $\log U \simeq -2.6$ but develops a long tail toward higher values $\log U \simeq -(1-2)$.

Changes in the pressure and the effective covering factor result from a preference for enhanced O/H. The strong UV [O III] $\lambda\lambda 1660, 1666$ are detected, but there are interesting upper limits on the optical [O III] $\lambda\lambda 4959, 5007$ and H Balmer lines. [O III] $\lambda\lambda 4959, 5007$ are collisionally suppressed above $n_e = 6.4 \times 10^5 \text{ cm}^{-3}$ (Draine 2011a), such that increased P will reduce the optical doublet relative to the UV doublet. By contrast, enhancing the O abundance dramatically enhances the optical [O III] doublet more than the UV [O III] doublet, likely owing to increased line cooling in a metal-rich gas preferentially suppressing the UV forbidden lines. These effects manifest as a positive correlation between P and O/H, and a negative correlation between x and O/H (Fig. 8). Since the oxygen lines increase with O/H, a solution with increased O/H is preferred to explain strong [O III] and [O II] without H Balmer detections. The covering factor must decrease to avoid overproducing oxygen lines. Because this enhances [O III] $\lambda\lambda 4959, 5007$ more than [O III] $\lambda\lambda 1660, 1666$, P and hence n_e must be increased to suppress the former.

The high $\log U$ tail appears in the posterior distribution due to a preference for enhanced He/H. At high $\log U$, emission lines from higher excitation ions (O III, N III, Ne III) are enhanced relative to lines of lower excitation ions (O II, Si III, Fe III). Increased He abundance, which consumes more He I ionizing photons ($h\nu > 24.6 \text{ eV}$), has the opposite effect that a He I zone forms behind the He II zone where the low excitation ions can be abundant. Hence, there is a positive cor-

relation between He/H and $\log U$ (Fig. 8), as the two approximately compensate for one another with the exception of He emission lines.

As we fix the stellar metallicity $Z = 0.25 Z_{\odot}$ in this model, fitting results indicate that the gas-phase oxygen is enhanced by $\sim 2-6$ fold, producing an O/H at roughly the solar value. C, N, Si and Ne relative to O are found to be similarly abundant as in the Base Model, but have increased abundances relative to H. This implies that the inferred low C/O, Ne/O and Si/O values may be a symptom of O enrichment rather than a deficiency in C, Ne and Si. We find that He is enhanced relative to H by $\sim 2-4$ fold compared to the prescription of Russell & Dopita (1992).

This model again requires y to be closer to zero than to unity, but with a broader posterior distribution, $y < 0.2$, enabled by the enhanced O/H (see correlation in Figure 8). This implies that the nebular emission should be mostly HI-obscured, but up to $\sim 20\%$ of it may still come directly from unobscured irradiated cloud surfaces. As we shall discuss later, this preference in y has important implications for the probable nebula geometry (Section 6.4).

Since the Chemically Anomalous Model is consistent with a wide range of $\log U$ values, we further test a model involving two ionized gas components, one with low $\log U < -1.5$ as found in the Base Model, and another with high $\log U > -1.5$. The high ionization parameter $\log U > -1.5$ can be explained by photoionization nebulae in wind-blown bubbles surrounding individual main sequence O stars at ~ 4 Myr, if the cluster interior is filled with dense self-shielding gas which could have condensed from wind and CCSN ejecta (see Figure 2 and Section 6.4.3). Assuming that all other physical parameters are the same for the two components, we find that significant processing of the total cluster ionizing output ($\gtrsim 10\%$) by a second high $\log U$ nebula is neither favored nor ruled out by data, with the other inferred physical parameters unaltered.

6. DISCUSSION

In this Section, we discuss the many implications of our fitting results for the dynamics, chemical composition, and astrophysical origin of Godzilla’s nebula. We will refer to our fitting results derived for the Chemically Anomalous Model as the favorable model.

6.1. Nebular Pressure and Ionization Parameter

The ionized gas excited in Godzilla appears extremely dense $n_e \sim 10^{7-8} \text{ cm}^{-3}$ and highly pressurized $P \sim 10^{11.5-12} \text{ K cm}^{-3}$. This result appears very robust to us. The tight lower limit on the C III] $\lambda 1908$ /[C III] $\lambda 1906$

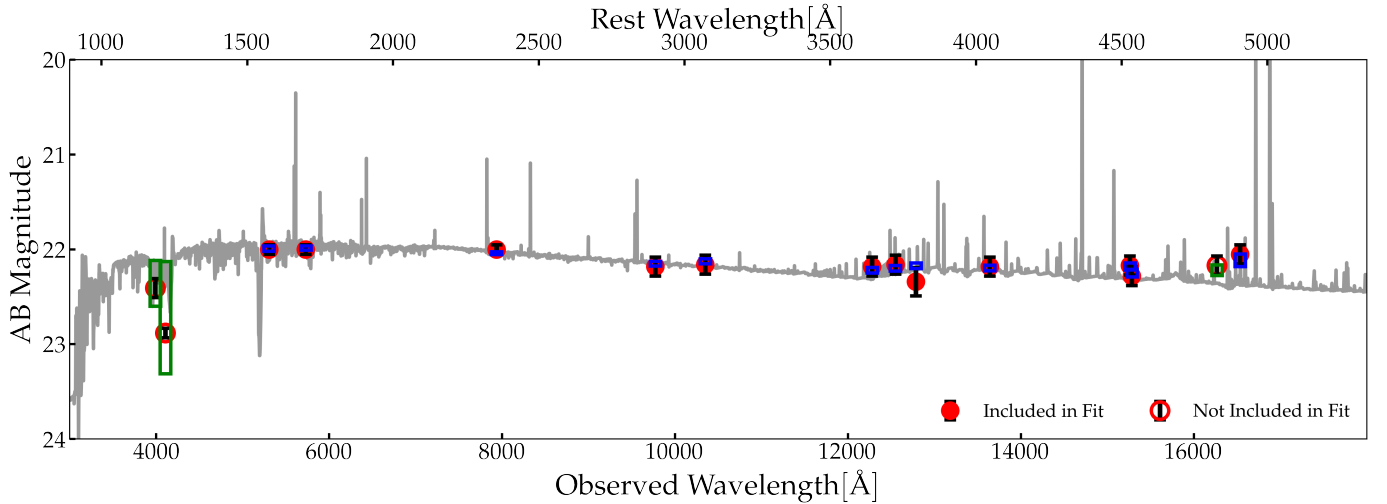


Figure 5. Best-fit SED (grey) from `CLOUDY` modeling with the Chemically Anomalous Model (Section 4.2). Co-plotted is the 68% C.I. range of the model predicted filter magnitude (open boxes) and the observed magnitude (circles with error bars). Two of the bluest filters F390W and F410M (open circles and green boxes) are excluded from the fit since the fluxes might have been significantly affected by Ly α line transfer and damping wing effects. The narrow-band F164N filter, significantly enhanced by H β , is not used due to potential flux calibration issues; however, its measured flux is consistent with model prediction.

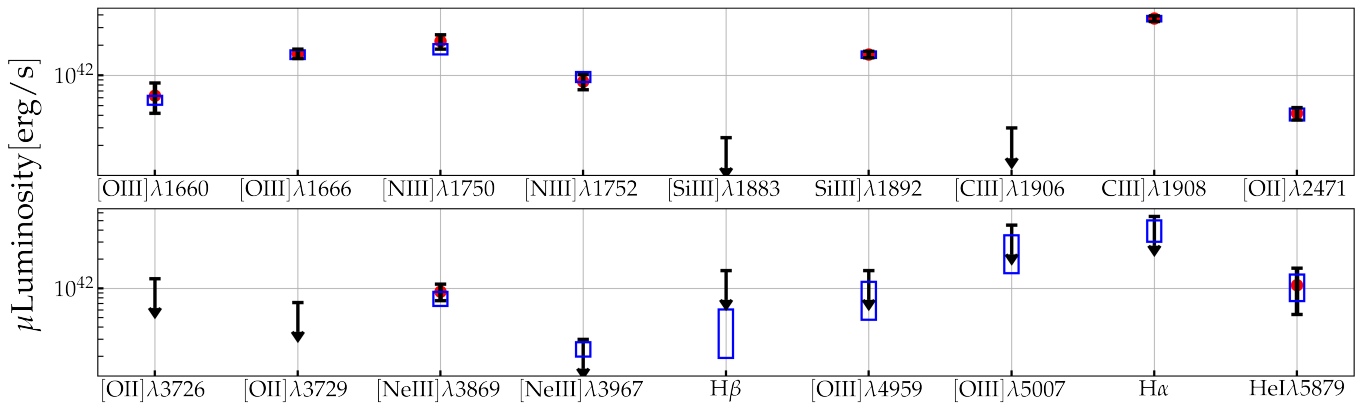


Figure 6. 68% C.I. for model predicted line fluxes (blue boxes) in the Chemically Anomalous Model (Section 4.2) and observed line fluxes from the MUSE and X-Shooter data (circles with errorbars). For non-detections, upper limits are plotted as downward arrows, which are implemented in fitting as strict upper limits.

alone implies $n_e > 10^6 \text{ cm}^{-3}$ (Vanzella et al. 2020b), but upper limits on [O III] $\lambda\lambda 4959, 5007$ in the presence of strong [O III] $\lambda\lambda 1650, 1666$ further requires $n_e > 10^7 \text{ cm}^{-3}$ to sufficiently suppress the former by electron collision. Interestingly, the high n_e reduces cooling via some collisionally excited metal lines such that dramatically increased O/H only causes a mild decrease in the electron temperature, a $\sim (10 - 15)\%$ drop in T_e for a five-fold increase in O/H. This leads to a unique situation where, despite a solar O/H, high excitation FUV lines like [O III] $\lambda\lambda 1660, 1666$ and [C III] $\lambda\lambda 1906, 1909$ remain strong, while at typical ISM densities these lines are not observed in star-forming regions with $Z \gtrsim 0.4 Z_\odot$ (Mingozzi et al. 2024).

6.2. Enrichment by Massive Star Winds: N and He

The localized, elevated N/O seen in Godzilla is significantly higher than in typical ISM environments (Fig. 10), including local HII regions (Pilyugin et al. 2012) and low- Z dwarf starbursts such as in the CLASSY survey (Berg et al. 2022). However, it is consistent with the N/O found in the LyC cluster in the same galaxy (Pascale et al. 2023), and bears similarity to a growing list of high- z N emitters, such as GN-z11 (Cameron et al. 2023; Senchyna et al. 2023) and CEERS-1019 (Marques-Chaves et al. 2024). P23 propose that the N enhancement seen in the LyC cluster likely arises from CNO-processed material ejected through massive star winds. We find this to be the most plausible explanation for Godzilla as well. Apart from the winds of classical WN

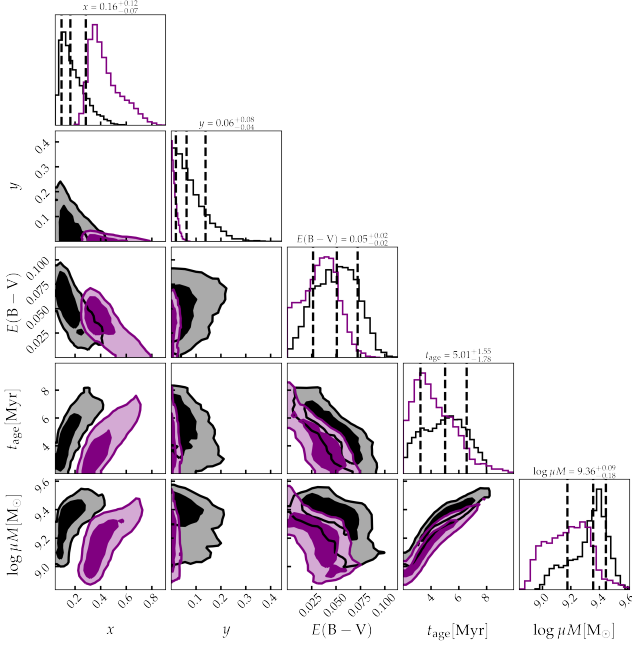


Figure 7. Posterior distributions for the star cluster parameters in the Chemically Anomalous Model (black) and the Base Model (purple). 1D histograms representing the posterior distributions are marked with the mean and 68% confidence intervals for the Chemically Anomalous Model (C.I.'s, dashed lines). 2D contours enclose 50% and 90% of the posterior samples. Refer to Table 4 for the 68% C.I.'s of the parameters.

stars, N-rich ejecta could also be provided through slow mass loss from non-conservative mass transfer between binary massive stars (de Mink et al. 2009), dense equatorial winds from fast rotating massive stars (Roy et al. 2022), continuum-driven dense winds from Very Massive Stars (Vink 2023), or even from supermassive stars that may form at the center of a dense super star cluster (Gieles et al. 2018; Charbonnel et al. 2023). All these could have happened in the cluster by 4 Myr.

Inside a sufficiently dense cluster, even fast line-driven winds from massive stars may be retained in the cluster potential from rapid loss of kinetic energy to radiative cooling (Wünsch et al. 2011, 2017b). Following the criteria of the semi-analytic analysis of Lochhaas & Thompson (2017a), Godzilla appears compact enough ($M_*/R > 10^5 M_\odot \text{pc}^{-1}$) that winds as fast as $v_w \sim 1000 \text{km s}^{-1}$ are expected to condense in the cluster.

Enhancement in He/H by a factor of $\sim 2-4$ than the ISM He abundance in Russell & Dopita (1992) is another piece of evidence for retained stellar wind material. Simultaneous N and He enrichment is not surprising given the inferred cluster age $> 3 \text{Myr}$. For a smaller t_{age} , winds from the Very Massive Stars would cause N enrichment without major He enrichment (e.g., Roy et al.

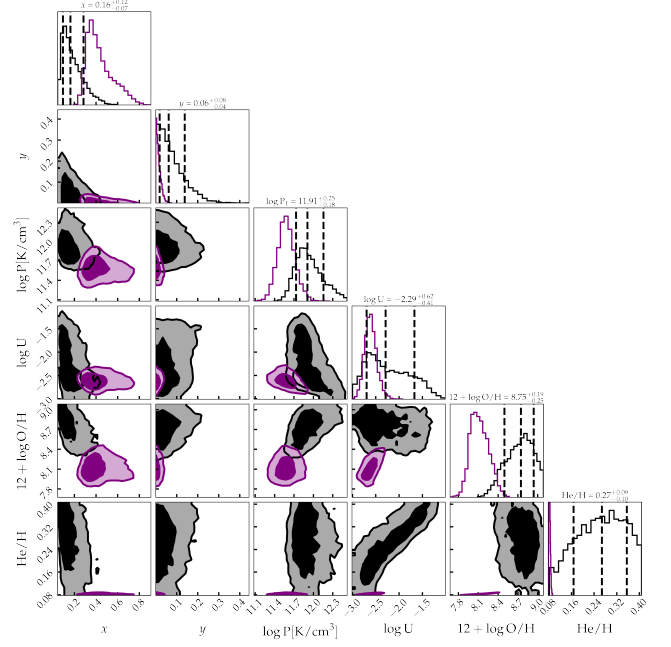


Figure 8. Posterior distributions for the physical parameters describing the nebula for the Chemically Anomalous Model (black) and for the Base Model (purple). Contours levels and histogram confidence intervals follow Fig. 7. The 68% C.I.'s of the parameters are tabulated in Table 4.

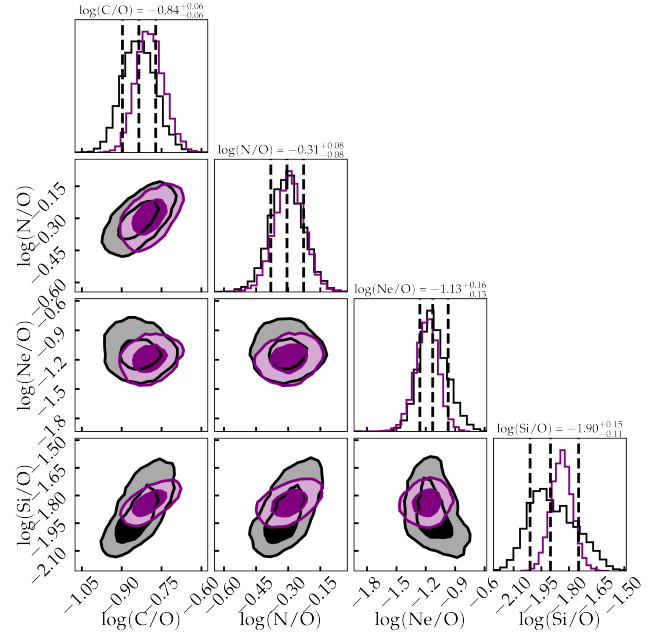


Figure 9. Posterior distributions for the gas-phase abundances of C, N, Ne and Si relative to O for the Chemically Anomalous Model (black) and the Base Model (purple). The 68% C.I.'s of the parameters are tabulated in Table 4.

2022; Vink 2023), while moderate He enhancement is expected to accompany N enhancement in the winds

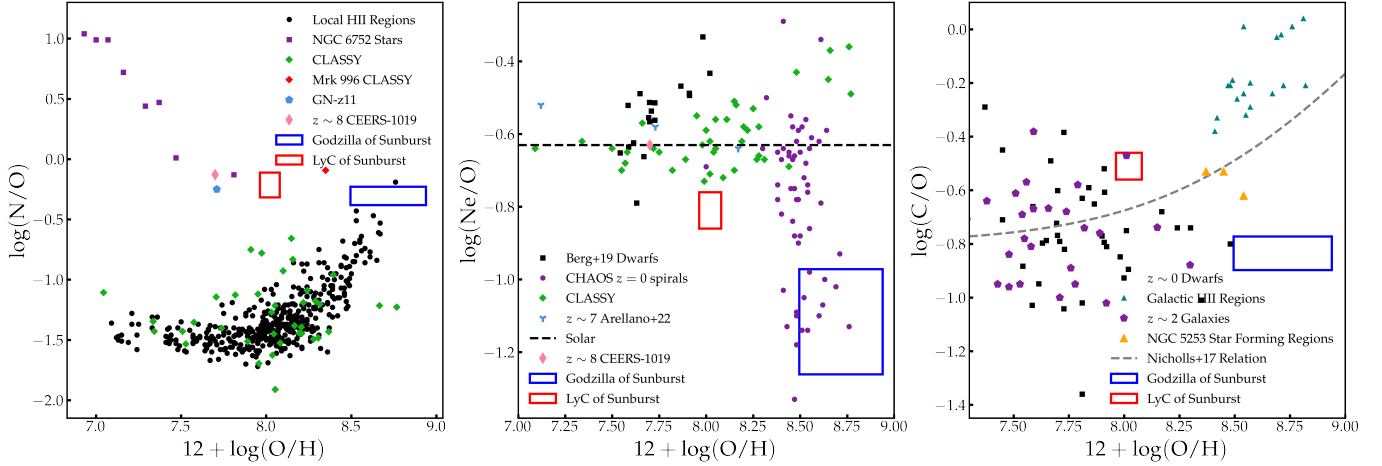


Figure 10. **Left:** Nitrogen abundances for Godzilla, the LyC cluster of Sunburst (Pascale et al. 2023), GN-z11 (Senchyna et al. 2023), the $z \sim 8$ galaxy CEERS-1019 (Marques-Chaves et al. 2024), stars of local globular clusters (NGC 6752 Carretta et al. 2005), local star forming galaxies (Berg et al. 2022; Stephenson et al. 2023, CLASSY), and local HII regions in SDSS galaxies (Pilyugin et al. (2012)). **Middle:** Neon abundance of Godzilla compared to local star-forming galaxies from CLASSY and Berg et al. (2019), star-forming regions of M33 from (Rogers et al. 2022, CHAOS), the $z \sim 7$ galaxies of Arellano-Córdova et al. (2022), and the solar value $\log(\text{Ne}/\text{O}) = 0.63 \pm 0.05$ (Asplund et al. 2021). **Right:** Carbon abundance of Godzilla compared to local star-forming galaxies (Berg et al. 2016, 2019; Senchyna et al. 2017; López-Sánchez et al. 2007), galactic HII regions (Arellano-Córdova et al. 2020), a sample of $z \sim 2$ galaxies from the literature (Pettini et al. 2000; Fosbury et al. 2003; Erb et al. 2010; Christensen et al. 2012; Bayliss et al. 2014; James et al. 2014; Stark et al. 2014; Steidel et al. 2016; Vanzella et al. 2016; Amorín et al. 2017; Berg et al. 2018; Rigby et al. 2018) and the empirical relation derived by Nicholls et al. (2017). Figures are recreated following Senchyna et al. (2023), Berg et al. (2019), and Arellano-Córdova et al. (2022), and error bars are omitted for visual clarity.

of evolved He stars (e.g., Meynet et al. 2006; Decressin et al. 2007).

6.3. Enrichment by CCSNe: C/O, Si/O, and Ne/O

Another marked event is the onset of CCSNe when the star cluster evolves beyond 3 Myr. Godzilla shows a low gas-phase $\log(\text{C}/\text{O}) = -0.8$ compared to the solar value and to HII regions at the similar O/H (approximately solar). However, this C/O value is more consistent with star-forming regions of gas-phase $Z \lesssim 0.25 Z_{\odot}$ at Cosmic Noon (Fig. 10; Garnett et al. 1995; Berg et al. 2016; Nicholls et al. 2017; Berg et al. 2019). Berg et al. (2016) and Berg et al. (2019) observe a trend in C/O versus O/H in local and intermediate- z star-forming galaxies, which appears mostly flat at SMC-like metallicities or lower, but shows a strong upturn at higher metallicities (Figure 7 of Berg et al. 2016 and Figure 10 of Berg et al. 2019). Berg et al. (2019) posit that this trend can be explained by a model of bursty star formation, where prompt CCSNe first enhance the gas-phase oxygen to produce a mostly flat C/O trend with metallicity. Then, pseudo-secondary production of carbon from low-mass asymptotic giant branch (AGB) stars, together with Z -dependent winds of evolved stars relevant only for metallicities greater than the SMC value, is responsible for an upward trend of C/O versus O/H. This provides a plausible explanation for Godzilla, in

which at an age of $\sim 4\text{--}6$ Myr the first CCSNe significantly enrich the cluster gas with oxygen, leading to a low gas-phase C/O. Godzilla, however, shows enhanced O/H and hence C/H, relative to the galaxies of the Berg et al. (2019) sample. This can be explained by the different length scales of enrichment. On the galactic scale, the CCSNe ejecta are likely diluted in the ISM, leading to sub-solar O/H values. The localized nebula gas of Godzilla may consist of, either entirely or significantly, the stellar ejecta, thus exhibiting a solar-like gas-phase O/H. Because the location of the upturn observed in the C/O versus O/H trend is set by the stellar metallicity, the gas-phase C/O of Godzilla would be consistent with the values for galaxies at sub-solar metallicities despite the inferred solar value for gas-phase O/H.

To further investigate whether the nebula of Godzilla is heavily enriched by massive star winds and CCSNe ejecta, we draw comparison to the models of Mollá & Terlevich 2012 (hereafter MT12), who calculated the element abundances for the cumulative wind and CCSNe ejecta of a fiducial $M_{\star} = 10^6 M_{\odot}$ star cluster across the stage of early evolution up to an age of 20 Myr, assuming *complete* ejecta retention without mixing with the ISM.

This is intended to be a qualitative comparison, as there are numerous differences between our cluster model for Godzilla and the models assumed in MT12,

Table 4. Fitting results for the Base Model and the Chemically Anomalous Model. In the Base Model the gas-phase oxygen abundance is identified with the stellar metallicity, while in the Chemically Anomalous Model we fix the stellar metallicity to $0.25 Z_{\odot}$ but allows gas-phase O and He abundances to vary in `Cloudy` calculations. Pressures are in units of K cm^{-3} , photon fluxes ($\Phi(\text{H}^0)$) in units of $\text{cm}^{-2} \text{s}^{-1}$, and the characteristic nebula radii (R) in units of cm. The magnification factor of Godzilla, μ , is likely large $\sim \mathcal{O}(100)$ but uncertain.

Parameter	Base Model	Chem. Model
χ^2_{ν}	0.52	0.39
χ^2	9.36	6.63
$E(B - V)$	$0.02^{+0.02}_{-0.02}$	$0.05^{+0.02}_{-0.02}$
$\log Z_{\star}^a$	$-2.29^{+0.16}_{-0.12}$	-2.3
t_{age} [Myr]	$4.03^{+1.78}_{-1.22}$	$5.01^{+1.55}_{-1.78}$
$\log U$	$-2.61^{+0.13}_{-0.011}$	$-2.29^{+0.62}_{-0.41}$
$\log P$	$11.56^{+0.14}_{-0.12}$	$11.91^{+0.25}_{-0.18}$
$\log(\mu M_{\star})$	$9.29^{+0.11}_{-0.16}$	$9.36^{+0.09}_{-0.18}$
$\log(\mu Q(\text{H}^0))$	$55.54^{+0.17}_{-0.25}$	$55.54^{+0.23}_{-0.27}$
$\log \Phi(\text{H}^0)$	$15.22^{+0.16}_{-0.15}$	$15.89^{+0.38}_{-0.34}$
$\log(R\mu^{1/2})$	$19.60^{+0.12}_{-0.13}$	$19.25^{+0.20}_{-0.17}$
x	$0.40^{+0.15}_{-0.09}$	$0.16^{+0.12}_{-0.07}$
y	$0.01^{+0.02}_{-0.01}$	$0.06^{+0.08}_{-0.04}$
$\log(\text{C}/\text{O})$	$-0.79^{+0.05}_{-0.05}$	$-0.84^{+0.06}_{-0.06}$
$\log(\text{N}/\text{O})$	$-0.30^{+0.07}_{-0.07}$	$-0.31^{+0.08}_{-0.08}$
$\log(\text{Ne}/\text{O})$	$-1.20^{+0.11}_{-0.12}$	$-1.13^{+0.16}_{-0.13}$
$\log(\text{Si}/\text{O})$	$-1.84^{+0.06}_{-0.05}$	$-1.90^{+0.15}_{-0.11}$
$12 + \log(\text{O}/\text{H})$	$^b 8.09^{+0.17}_{-0.11}$	$8.75^{+0.19}_{-0.25}$
He/H	$^c 0.08^{+0.00}_{-0.00}$	$0.27^{+0.09}_{-0.10}$

^aWhere $\log Z_{\odot} = -1.85$

^bDerived from Z_{\star} , where $12 + \log(\text{O}/\text{H})_{\odot} = 8.69$.

^cDerived from Z_{\star} following [Russell & Dopita \(1992\)](#).

in addition to other underlying theoretical uncertainties. First, [MT12](#) used a Kroupa IMF ([Kroupa 2001](#)) with lower and upper mass cutoffs at $m_{\text{min}} = 0.15 M_{\odot}$ and $m_{\text{max}} = 100 M_{\odot}$ respectively, and used stellar evolution tracks that do not account for the effects of stellar rotation or binary evolution. Additionally, our Godzilla model has $Z = 0.25 Z_{\odot}$ for the stars, while the set provided in [MT12](#) with the closest stellar metallicity has $Z = 0.2 Z_{\odot}$. While $Z = 0.2 Z_{\odot}$ or $0.25 Z_{\odot}$ are well within our inference uncertainties and does not significantly change the incident stellar radiation, this is in a range of transition where the abundance of classical WR stars appears to depend sensitively on Z . Finally, we shall assume that the Ne and Si abundances of the wind shown in [Figures 11 and 12](#) follow from one-fifth the solar value, as [MT12](#) only provide Ne and Si yields

from CCSNe. Hence in the wind ejecta the Ne and Si masses are set by the H mass, assuming that hydrogen in the wind material has not been significantly depleted into He through nuclear burning.

We compare our inferred abundances for Godzilla to those derived by [MT12](#) in [Fig. 11](#) and [Fig. 12](#), which are shown relative to hydrogen and to oxygen, respectively. When compared to hydrogen, we find the abundances of He, C, N, O, Si and Ne are all consistent with the [MT12](#) predictions for complete retention of both wind and CCSN ejecta over the inferred cluster age. This supports the hypothesis that an order-unity fraction of Godzilla’s nebula gas is stellar ejecta. Given the sharp upturn in oxygen abundance after the onset of CCSNe at ~ 3.7 Myr in the [MT12](#) models, many of the abundances are only consistent within a short time window of $\sim 1 - 2$ Myr. However, this is consistent with the cluster age we infer from broad-band photometry and nebular emission lines.

Plotting the abundances relative to oxygen ([Fig. 12](#)), all abundances remain in good agreement with the [MT12](#) predictions, with the exception of Ne/O. In a broader context, ISM Ne/O measurements in star forming regions nearly ubiquitously show the solar value or are only mildly lower ([Henry & Worthey 1999](#); [Willner & Nelson-Patel 2002](#)). While $\log(\text{Ne}/\text{O}) < -1$ was reported for a number of low ionization regions measured in the CHAOS sample of M33 (see [Fig. 10](#); [Rogers et al. 2022](#)), those exhibited large measurement uncertainties and are qualitatively different environments than a young massive star cluster.

Rather, we suggest that a sub-solar Ne/O may be typical in the early evolution of super star clusters as a consequence of CCSNe yields for progenitors of high ZAMS masses. At an inferred age ~ 5 Myr, Godzilla uniquely probes CCSNe yields within only 1–2 Myr of CCSN onset when only stars $m_{\text{ZAMS}} \gtrsim 30\text{--}40 M_{\odot}$ have ended their lives ([Bressan et al. 2012](#)). While tables provided by [MT12](#) show solar or even super-solar Ne/O values at these young ages (drawing from yield models of [Woosley et al. 1993](#) and [Woosley et al. 1995](#)), Ne/O of massive stars is subject to significant theoretical uncertainty. For example, [Limongi & Chieffi \(2018\)](#) predict solar and sub-solar Ne/O from massive stars at low metallicity, and the $\log(\text{Ne}/\text{O})$ values are significantly lowered below -1 in rotating star models, a feature not accounted for in the yield models used by [MT12](#). More exotic sources, such as metal-free massive star hypernovae ([Grimmett et al. 2018](#)) or high mass pair-instability SNe ([Heger & Woosley 2002](#)) have also been predicted to produce sub-solar Ne/O ([Ji et al. 2024](#)).

To investigate possible reasons for the reduced Ne/O, we take the MT12 ejecta models but exclude Ne and Si yields from CCSNe. We find that this resolves the tension in Ne/O and may also improve the agreement for Si/O. This may be evidence that CCSNe of high m_{ZAMS} progenitors have deficient Ne/O compared to their lower m_{ZAMS} counterparts. While Ne and O are both abundant in the Ne-Mg-O shell of the pre-SN star, Ne may be depleted via photo-disintegration, converting to O pre-SN or during explosive nucleosynthesis (Boccioli & Roberti 2024). This may also be related to a scenario in which the Ne-Mg-O and Si-S shells interior to the pre-SN star do not successfully get ejected while the more exterior C-O shell is ejected, although this may not provide enough O enhancement relative to C to match the observed sub-solar C/O value (Woosley et al. 2002).

Overall, and despite the various measurement and theoretical uncertainties, we find that the unusual gas-phase abundances we infer for Godzilla using the Chemically Anomalous Model can be remarkably well-explained by a model in which the nebula is a full mixture of winds and CCSN ejecta from stars with $m_{\text{ZAMS}} \gtrsim 30\text{--}40 M_{\odot}$. This interpretation is consistent with the inferred cluster age $\sim 4\text{--}6$ Myr.

6.4. Nebula Geometry and Dynamics

In this Section, we discuss the nebula geometry of Godzilla and the possible underlying dynamical reasons.

6.4.1. Spherical Shell Enclosing Stars

The simplest geometry would be a spherical shell of nebular clouds surrounding the entirety of the ionizing sources at some distance R_{sh} , with an area covering factor $x \simeq 0.1\text{--}0.2$. In P23, we found that this simple geometry can explain the spectra of the LyC cluster. For $\log P = 11.9$, $\log U = -1.5$ and $\text{He}/\text{H} = 0.35$ (Figure 8), we require $n_e \sim 10^7 \text{ cm}^{-3}$, and the characteristic ionizing flux is $\log \Phi(\text{H}^0) = 15.9$. Comparing this to the BPASS prediction of ionizing photon production rate, we obtain $\log(R\mu^{1/2}) = 19.3$ [cm] or $R_{\text{sh}} \simeq 0.4 \text{ pc } \mu_{300}^{-1/2}$. While such a compact size would be implausible for the entirety of a star cluster that is more massive than $10^6 M_{\odot}$, the shell would only have to enclose the majority of the ionizing stars which may aggregate toward the cluster center (Sung & Bessell 2004; Stolte et al. 2002; Crowther et al. 2010; Pang et al. 2013), but not necessarily all cluster stars. While it would help to place the major ionizing sources all within $\simeq 0.4 \text{ pc}$ by invoking primordial mass segregation, given the large cluster mass and its age $\sim 4\text{--}6$ Myr (so that the most massive stars have died), this compactness is still quite extreme.

Alternatively, the shell may have a 100% area covering but only encloses $x = (10\text{--}20)\%$ of the cluster’s ionizing

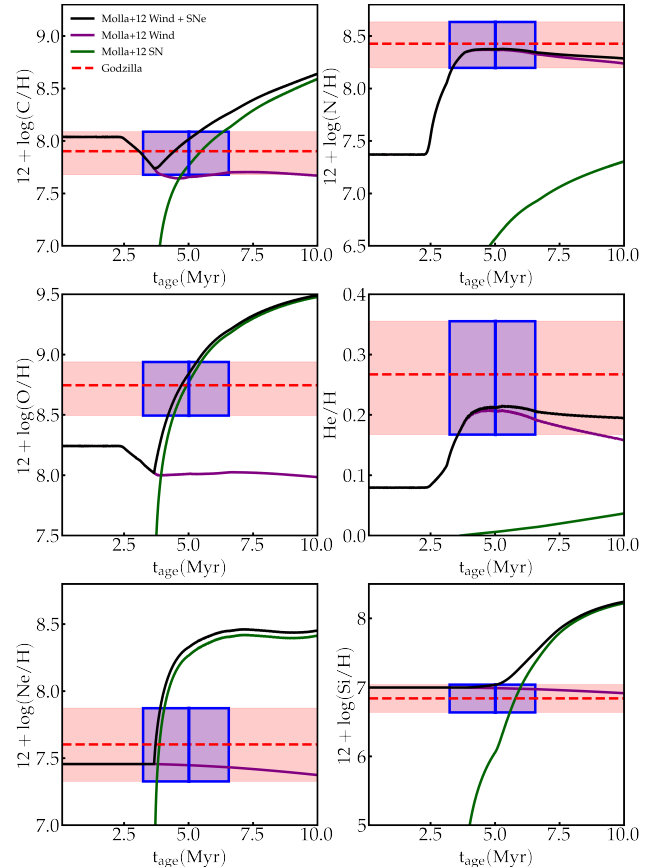


Figure 11. Evolution of the abundances of accumulated wind and CCSN ejecta. Model predictions from MT12 (black solid lines) are compared to abundances inferred for Godzilla with the Chemically Anomalous Model (dashed red lines and red swaths represent the median and 68% confidence interval respectively). The relative contributions of winds and SN to the total ejecta are plotted in purple and green respectively. We note that these represent the contribution to the abundance of the cumulative ejecta and not the abundances of the wind or SN themselves. For reference, we also plot for cumulative ejecta with CCSN yields of Ne and Si excluded (black dashed lines). We find the cluster age $\sim 4\text{--}6$ Myr (blue box) inferred from the Chemical Anomalous Model, is in good agreement with the MT12 predictions, such that Godzilla’s nebula may be an order-unity condensation of wind and CCSN ejecta.

output. This, however, would require an even smaller shell radius $R_{\text{sh}} = 0.18 \text{ pc } \mu_{300}^{-1/2} (x/0.2)^{1/2}$. A compact gas shell enclosing a hollow cavity in the cluster center seems geometrically unnatural. We note, however, that in case the shell is thick this geometry would resemble our most favored geometry to be discussed in Section 6.4.3, and the large hollow cavity could have been driven by a recent CCSN.

6.4.2. Shattered Clouds

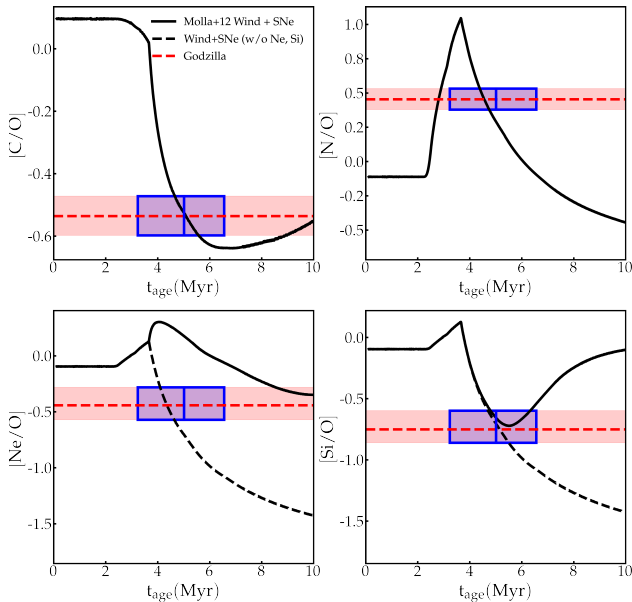


Figure 12. Same as Figure 11 but with abundances plotted relative to oxygen and normalized to the solar value. We find that the MT12 predictions agree with the inferred abundances of Godzilla at ~ 4 – 6 Myr, with the exception of Ne/O, which only shows agreement if the CCSN Ne yield is significantly reduced (dashed line).

A second possibility is that the nebula emission comes from a population of shattered, self-shielding clouds, which are hovering within a spherical volume of radius $R_c \simeq 0.4 \text{ pc } \mu_{300}^{-1/2}$ that encloses nearly all of the cluster’s ionizing output, but have an area covering factor $x \simeq 0.1$ – 0.2 . The compactness of this volume may be explained again by mass segregation.

Similar to the geometry discussed in Section 6.4.1, we have to explain the high pressure $\log P \simeq 11.9$ of the nebula gas. Since we inferred $\log U < -1$, direct ionizing radiation pressure is insufficient (Yeh & Matzner 2012),

$$P_{\text{rad}} = 6 \times 10^{10} \text{ K cm}^{-3} \left(\frac{\Phi(\text{H}^0)}{10^{15.9} \text{ s}^{-1} \text{ cm}^{-2}} \right) \left(\frac{\langle h\nu \rangle_{\text{ion}}}{20 \text{ eV}} \right), \quad (1)$$

where $\langle h\nu \rangle_{\text{ion}}$ is the average energy of the ionizing photons. Thus, thermal pressure from an intracloud hot gas component with $\log P_{\text{hot}} \simeq 11.9$ needs to confine the clouds.

Can a global hot cluster wind provide the sufficient pressure? In a simple picture, mass and kinetic energy output from individual stellar winds and CCSNe merge to drive a hot cluster wind (Chevalier & Clegg 1985; Cantó et al. 2000; Wünsch et al. 2011; Silich et al. 2011). Estimating from BPASS (v2.2), the total stellar mass loss rate is $\dot{M}_* \approx 0.01 M_\odot \text{ yr}^{-1}$ per $10^6 M_\odot$ of stars, including wind and SN mass ejection. Taking a specific

CCSN rate at $t_{\text{age}} \sim 5$ Myr of $\Gamma_{\text{SN}} \approx 5 \times 10^{-10} \text{ yr}^{-1} M_\odot^{-1}$ and an explosion energy $E_{\text{SN}} = 10^{51} \text{ erg}$ per CCSN, the mechanical luminosity due to CCSNe is $L_{\text{mech,SN}} \approx 1.6 \times 10^{40} \text{ erg s}^{-1}$ per $10^6 M_\odot$ of stellar mass. Including wind mass loss at $v_w \approx 2000 \text{ km s}^{-1}$ causes at most a factor of two increase in the total mechanical luminosity, reaching $L_{\text{mech,tot}} \approx 3 \times 10^{40} \text{ erg s}^{-1}$ per $10^6 M_\odot$ of stellar mass.

Assuming no radiative loss, we find a pressure for the cluster hot gas:

$$P_{\text{hot}} \approx 5 \times 10^{11} \text{ K cm}^{-3} \left(\frac{M_{*,6}}{6} \right) \left(\frac{R_c}{0.4 \text{ pc}} \right)^{-2} \times \left(\frac{L_{\text{mech,tot}}}{3 \times 10^{40} \text{ erg s}^{-1}} \right)^{1/2} \left(\frac{\dot{M}_*}{0.01 M_\odot \text{ yr}^{-1}} \right), \quad (2)$$

where $M_{*,6} = M_*/(10^6 M_\odot)$ and R_c is the radius of the cluster core region where the hot gas is fully thermalized. We obtain a sufficiently high value because we have used a compact radius $R_c = 0.4 \text{ pc}$ for thermalization, which we deem quite extreme.

However, we emphasize that the above analysis is very optimistic because it assumes maximal thermalization without radiative loss. Any radiative loss lowers the hot gas temperature and the pressure. Taking $\log P_{\text{hot}} = 11.9$, the hot gas needs to have a high density $n_{\text{hot}} = 8 \times 10^4 \text{ cm}^{-3}$ ($10^7 \text{ K}/T_{\text{hot}}$) and hence a short cooling time $t_{\text{cool}} \simeq 60 \text{ yr } (T_{\text{hot}}/10^7 \text{ K})^{1.7} (n_{\text{hot}}/10^5 \text{ cm}^{-3})$ (Draine 2011a). This is not longer than the timescale of streaming across the core region $t_{\text{cr}} = R_c/v_{\text{hot}} = 400 \text{ yr } (R_c/0.4 \text{ pc})/(v_{\text{hot}}/1000 \text{ km s}^{-1})$, and is shorter than the typical time separation between successive CCSNe $\sim 1/(\Gamma_{\text{SN}} M) \simeq 300 \text{ yr } (\Gamma_{\text{SN}}/5 \times 10^{-10} \text{ yr}^{-1} M_\odot^{-1})^{-1} (M/6 \times 10^6 M_\odot)^{-1}$, even if all CCSNe occur at the cluster center. Therefore, such a compact hot cluster gas component seems unstable to radiative cooling.

Importantly, we expect $y \simeq 1/2$ for the shattered-cloud geometry, since the dense clouds would naturally have a more or less isotropic distribution about the cluster center. A y value that strongly hints at the HI-obscured geometry, $y < 0.2$, does not favor this geometry.

6.4.3. HII Bubbles within Condensed Gas

Following previous discussions, dense cluster hot gas inevitably enters the regime of catastrophic radiative cooling (Silich et al. 2004; Wünsch et al. 2011; Gray et al. 2019; Danekhar et al. 2021; Lochhaas & Thompson 2017b; Wünsch et al. 2017a), so that it would fail to blow out at all. It is found in hydrodynamic simulations that in this regime, gas undergoes rapid radiative

cooling and accumulates at the cluster center (Wünsch et al. 2017a).

Motivated by this insight, we propose a different nebula geometry (Figure 2): catastrophically cooled cluster gas expelled from the massive stars has accumulated in the cluster core since the beginning of the cluster evolution. This gas is dense enough that it self-shields against ionizing photons even though it is interspersed between the O stars. If the gas is not dusty (no significant dust reddening is seen toward Godzilla), its neutral interior can still be heated due to photoionization of metals by the intense UV light and hence stay warm at a few thousand Kelvin. The nebular emission may then come from ionization-bounded HII bubbles surrounding individual O stars which are embedded in self-shielding cluster gas that fills the cluster core.

This scenario is motivated by several hints. First, special chemical abundances are indicative of a nebula gas origin from retained wind and CCSN ejecta; catastrophic cooling may first cause the wind material to accumulate in the cluster core, while the later CCSN ejecta may be trapped within. Second, individual ionization-bounded HII bubbles can be very compact, which allows for high $\Phi(\text{H}^0)$ values, as we will show. Finally, fitting preference for a small y value helps explain the weakness of H Balmer lines and indicates a high fraction of nebula emission that is affected by significant HI columns along the line of sight.

Each individual O star with wind mass loss rate \dot{M}_w , wind velocity v_w and ionizing photon rate S_0 blows a bubble around it within the dense cluster gas. The bubble feels a “headwind” of the ambient cluster gas due to the relative velocity between the star and the ambient gas flow. With efficient radiative cooling, shell gas can form from this interaction (Scherer et al. 2016; Titova et al. 2021). Accounting for wind and radiation pressures, the bubble radius R_b along the stagnation line can be estimated from $P = (4\dot{M}_w v_w + \Phi_0 \langle h\nu \rangle_{\text{ion}})/(4\pi R_b^2)$, where $\langle h\nu \rangle_{\text{ion}} \approx 20 \text{ eV}$ is the typical energy of the ionizing photons and a factor of 4 in front of $\dot{M}_w v_w$ accounts for the thickness of the shocked wind. The bubble has a compact size:

$$R_b = 170 \text{ AU} \left(\frac{1 + \zeta}{2.5} \right)^{\frac{1}{2}} \left(\frac{S_0}{10^{48.5} \text{ s}^{-1}} \right)^{\frac{1}{2}} \left(\frac{\langle h\nu \rangle_{\text{ion}}}{20 \text{ eV}} \right)^{\frac{1}{2}} \times \left(\frac{P}{10^{11.9} \text{ K cm}^{-3}} \right)^{-\frac{1}{2}}, \quad (3)$$

where we define $\zeta = (4\dot{M}_w v_w)/(S_0 \langle h\nu \rangle_{\text{ion}})$. The fiducial values, $S_0 = 10^{48.5} \text{ s}^{-1}$, $\dot{M}_w = 10^{-7} M_\odot \text{ yr}^{-1}$, $v_w = 2000 \text{ km s}^{-1}$ and hence $\zeta = 1.5$, are chosen for median O stars that contribute to the ionizing output

at $t_{\text{age}} = 5 \text{ Myr}$ ($m_{\text{ZAMS}} \simeq 25 M_\odot$) (Bressan et al. 2012). If instead $t_{\text{age}} = 4 \text{ Myr}$, we have $S_0 = 10^{49} \text{ s}^{-1}$, $\dot{M}_w = 10^{-6.5} M_\odot \text{ yr}^{-1}$ but again with $\zeta = 1.5$, for median O stars with $m_{\text{ZAMS}} \simeq 40 M_\odot$, which corresponds to $R_b = 300 \text{ AU}$. Since the HII bubbles are much smaller than the typical separation between O stars within the cluster, their total volume filling fraction is tiny.

In the ionized gas where nebular emission lines form, we have $P \approx 2n_e k_B T_e$. For the ionizing photon rate S_0 from one O star, the ionization parameter is $U = S_0/(4\pi R_b^2 n_e c)$. This gives $U \approx (2k_B T_e)/(\langle h\nu \rangle_{\text{ion}}(1 + \zeta))$, or numerically

$$U = 10^{-1.5} \left(\frac{1 + \zeta}{2.5} \right)^{-1} \left(\frac{T_e}{10^4 \text{ K}} \right) \left(\frac{\langle h\nu \rangle_{\text{ion}}}{20 \text{ eV}} \right)^{-1}, \quad (4)$$

which is insensitive to the exact value of the ambient pressure. This log U value is higher than what is inferred from the Base Model, but aligns more with solutions of elevated He/H found with the Chemical Anomalous Model (Figure 8). There is uncertainty in this estimation due to the anisotropic structure of the HII bubble given the motion of the O star relative to the cluster gas (e.g., Mackey 2023). We also caution about the uncertainty that the hot ionized bubbles could be larger with a lower log U value. It may be that some of these large bubbles are driven by ongoing SNRs from recent CCSNe (invoked to drive supersonic turbulence), a high-density, scaled-down analog of what happens to the multi-phase ISM in the Galaxy (McKee & Ostriker 1977).

We suggest that the stellar ejecta accumulated in the cluster core is in a state of supersonic turbulence, analogous to giant molecular clouds. Maintained by UV heating, the gas is only at a few thousand K, and its sound speed c_s , at several km s^{-1} , is smaller than the virial velocity in the cluster potential, which easily reaches tens of km s^{-1} for $M_\star \sim 10^6 M_\odot$ and $R \sim 1 \text{ pc}$. Supersonic turbulence is therefore required to support this gas, at least for one or several Myr, against gravitational collapse which would quickly turn it into stars. The turbulence velocity should be on the order of the virial velocity in the cluster core.

Most of the volume is filled with the turbulent HI gas. For a large turbulence Mach number $\mathcal{M} = u/c_s$ (where u is the turbulence velocity on the largest scale), the gas is highly inhomogeneous (Hennebelle & Chabrier 2008; Hopkins 2012). The individual HII bubbles around O stars mostly probe the volume-weighted median density n_V , which should be high enough to provide the ram

pressure in the “headwind”:

$$n_V \simeq \frac{P}{m_p u^2} = 3 \times 10^6 \text{ cm}^{-3} \times \left(\frac{P}{10^{11.9} \text{ K cm}^{-3}} \right) \left(\frac{u}{50 \text{ km s}^{-2}} \right)^{-2}. \quad (5)$$

The typical HI column density in front of the nebular source is $N_{\text{HI}} \simeq n_V R_g = 3 \times 10^{24} \text{ cm}^{-2} (n_V/10^{6.5} \text{ cm}^{-3}) (R_g/0.3 \text{ pc})$. Viewing from the outside, the FUV sources inside the HI gas is analogous of an extremely damped Ly α system. In fact, for $N_{\text{HI}} = 3 \times 10^{24} \text{ cm}^{-2}$, the Ly α damping wing absorption equivalent width is huge $\sim 1000 \text{ \AA}$, which means FUV flux in the wavelength range of H Lyman series should be completely attenuated. However, this does not necessarily contradict data, as in our model FUV sources embedded within the retained HI gas make up a small fraction (e.g. $\lesssim 10\%$) of the cluster’s total FUV flux. A lot more FUV sources are expected to be exterior to the HI gas; ionizing radiation are expected to be more concentrated than FUV radiation in dense young star clusters (Kim et al. 2023).

A more important, fundamental difference between damped Ly α systems and the geometry we consider is that for the former photons are scattered out of line of sight, while for Godzilla photons do have to eventually emerge from the HI gas cloud somewhere. Accounting for photons scattered back into the line of sight therefore reduces the trough width. Indeed, F390W and F410M fluxes appear to be moderately deficient but far from being completely attenuated (Figure 5).

According to the theory of supersonic turbulence, the mean density \bar{n} should be larger than n_V by a factor $e^{\sigma_s^2/2}$ (Hennebelle & Chabrier 2008; Padoan et al. 2014), where $\sigma_s^2 \simeq 4\text{--}5$ for $\mathcal{M} \simeq 10$ (Federrath et al. 2021). Thus, \bar{n} should be a factor of 10 larger than Eq. (5).

The retained gas core radius R_g may be a fraction of the cluster size since we infer a small covering factor $x \simeq 0.2$. The gas mass required is

$$M_g \approx 9 \times 10^4 M_\odot \left(1 + \frac{4\text{He}}{\text{H}} \right) \left(\frac{\bar{n}}{10^{7.5} \text{ cm}^{-3}} \right) \left(\frac{R_g}{0.3 \text{ pc}} \right)^3. \quad (6)$$

For a cluster mass $M_\star = 6 \times 10^6 M_\odot / \mu_{300}$ and if R_g is a fraction of a parsec, there is sufficient wind mass loss and CCSN ejecta to account for $M_g \lesssim 10^5 M_\odot$.

If we identify the turbulence outer scale with the radial extent of the accumulated gas cloud R_g , the sonic scale (Padoan 1995),

$$l_s = \left(\frac{c_s}{u} \right)^2 R_c = 617 \text{ AU} \left(\frac{R_g}{0.3 \text{ pc}} \right)^2 \left(\frac{\mathcal{M}}{10} \right)^{-2}, \quad (7)$$

is larger or comparable to the typical HII bubble size R_b (see Eq. (3)). Indeed, the “headwind” does not behave clumpy before colliding with the O star wind.

The SNR expands into the cluster gas at the volume-weighted median density n_V . For $n_V \gtrsim 10^6 \text{ cm}^{-3}$, the SNR can fail to break out of the condensed cluster gas before it dissipates, even for R_g as small as a fraction of a parsec. This allows the condensed gas to stay in the cluster potential, and injects a small fraction of the explosion energy into the gas to maintain turbulence. We will discuss this in Section 6.5.

We note that the geometry of individual HII bubbles embedded within turbulent HI gas can explain the preference for a small y value. There should still be ionizing sources beyond the radius R_g , which illuminate the cluster gas cloud from the outside. A y value close but not equal to zero may account for such non-HI-obscured contributions. This is an advantage of this model compared to the scenario of shattered dense clouds with a low area covering factor. We believe this unusual geometry best describes Godzilla in reality.

6.5. SN Driving of Turbulence

The state of supersonic turbulence is highly dissipative, radiating away the bulk of the flow energy on the order of the turnover time of the largest eddy, which should be on the order of the dynamic time (which is much shorter than $\sim \text{Myr}$). The energy dissipation rate is estimated to be

$$\begin{aligned} \left(\frac{dE}{dt} \right)_{\text{turb}} &\sim \frac{u^2}{2} \left(1 + \frac{4\text{He}}{\text{H}} \right) m_p \bar{n} \frac{4\pi}{3} R_g^3 \left(\frac{R_g}{u} \right)^{-1} \\ &\simeq 1 \times 10^{40} \text{ erg s}^{-1} \left(1 + \frac{4\text{He}}{\text{H}} \right) \left(\frac{\bar{n}}{10^{7.5} \text{ cm}^{-3}} \right) \\ &\times \left(\frac{R_g}{0.3 \text{ pc}} \right)^2 \left(\frac{u}{50 \text{ km s}^{-1}} \right)^3. \end{aligned} \quad (8)$$

We surmise that supersonic turbulence can be sustained by CCSNe after $t_{\text{age}} \simeq 3 \text{ Myr}$, at least when all CCSNe occur well within the retained gas. The bulk of the CCSN explosion energy will be radiated away, but a subdominant fraction of it can maintain gas turbulence.

Let us crudely estimate CCSN driving using the semi-analytic theory of a spherical symmetric SN remnant expanding into an ambient gas of uniform density n_V . The initial adiabatic expansion (Sedov 1959; Taylor 1950) creates a growing hot bubble of size as a function of time t

$$R_{\text{SNR}} \simeq 0.04 \text{ pc} \left(\frac{E_{\text{SN}}}{10^{51} \text{ erg}} \right)^{\frac{1}{5}} \left(\frac{n_V}{10^{6.5} \text{ cm}^{-3}} \right)^{-\frac{1}{5}} \left(\frac{t}{10 \text{ yr}} \right)^{\frac{2}{5}}. \quad (9)$$

A homologous Sedov-Taylor bubble has a temperature

$$T \simeq 6 \times 10^6 \text{ K} \left(\frac{E_{\text{SN}}}{10^{51} \text{ erg}} \right)^{\frac{2}{5}} \left(\frac{n_V}{10^{6.5} \text{ cm}^{-3}} \right)^{-\frac{2}{5}} \left(\frac{t}{10^2 \text{ yr}} \right)^{-\frac{6}{5}}. \quad (10)$$

Shortly after the hot bubble cools radiatively, a mass shell forms at the edge of the bubble. The evolution transitions to a pressure driven phase (Cox 1972; Chevalier 1974). To analytically estimate this transition point, we use a simple cooling function for $\Lambda(T) = 1.6 \times 10^{-19} \xi_m (T/\text{K})^{-1/2} \text{ erg cm}^3 \text{ s}^{-1}$, valid for the hot gas in the temperature range $10^5 < T/\text{K} < 10^{7.5}$. Here ξ_m is an order-unity parameter depending on the gas metallicity and $\xi_m \simeq 1$ at solar metallicity. For high n_V , the pressure driven phase is quickly reached at a time

$$t_{\text{PDS}} \simeq 3 \text{ yr} \left(\frac{E_{\text{SN}}}{10^{51} \text{ erg}} \right)^{\frac{3}{14}} \left(\frac{n_V}{10^{6.5} \text{ cm}^{-3}} \right)^{-\frac{4}{7}} \xi_m^{-\frac{5}{14}}, \quad (11)$$

with a shell radius

$$R_{\text{PDS}} \simeq 0.02 \text{ pc} \left(\frac{E_{\text{SN}}}{10^{51} \text{ erg}} \right)^{\frac{2}{7}} \left(\frac{n_V}{10^{6.5} \text{ cm}^{-3}} \right)^{-\frac{3}{7}} \xi_m^{-\frac{1}{7}}. \quad (12)$$

The shell has swept up ambient gas of mass $M_{\text{PDS}} \simeq (4\pi/3) m_p n_V R_{\text{PDS}}^3$, which is

$$M_{\text{PDS}} \simeq 6 M_{\odot} \left(\frac{E_{\text{SN}}}{10^{51} \text{ erg}} \right)^{\frac{6}{7}} \left(\frac{n_V}{10^{6.5} \text{ cm}^{-3}} \right)^{-\frac{2}{7}} \xi_m^{-\frac{3}{7}}. \quad (13)$$

The shell expands at a velocity

$$v_{\text{PDS}} = \frac{2 R_{\text{PDS}}}{5 t_{\text{PDS}}} \quad (14)$$

$$\simeq 3500 \text{ km s}^{-1} \left(\frac{E_{\text{SN}}}{10^{51} \text{ erg}} \right)^{\frac{1}{14}} \left(\frac{n_V}{10^{6.5} \text{ cm}^{-3}} \right)^{\frac{1}{7}} \xi_m^{\frac{3}{14}}.$$

At this point, the shell carries radial momentum (Ostriker & McKee 1988)

$$p_{\text{PDS}} = M_{\text{PDS}} \frac{9}{14} v_{\text{PDS}} \simeq 1.4 \times 10^4 M_{\odot} \text{ km s}^{-1} \quad (15)$$

$$\times \left(\frac{E_{\text{SN}}}{10^{51} \text{ erg}} \right)^{\frac{13}{14}} \left(\frac{n_V}{10^{6.5} \text{ cm}^{-3}} \right)^{-\frac{1}{7}} \xi_m^{-\frac{3}{14}}.$$

From this point onward, the SN remnant will expand substantially until the velocity of the wrinkled gas shell decreases to be comparable to the ambient turbulence velocity u . This process is close to but not perfectly momentum conserving. The final momentum injected

into the ambient gas, p_{SN} , is estimated to be only a few times larger than p_{PDS} , $\epsilon_p = p_{\text{SN}}/p_{\text{PDS}} = 2-3$, the remnant radius will have expanded by several fold $\epsilon_R = R_{\text{SN}}/R_{\text{PDS}} = 2-5$, and will have swept up a total mass $M_{\text{SN}} = \epsilon_R^3 M_{\text{PDS}}$ (Cioffi et al. 1988). The ratios ϵ_p and ϵ_R are expected to depend rather weakly on n_V (Cioffi et al. 1988).

The final kinetic energy injected into the ambient gas can be estimated as

$$K_{\text{SN}} = \frac{p_{\text{SN}}^2}{2 M_{\text{SN}}} = \frac{p_{\text{PDS}}^2}{2 M_{\text{PDS}}} \frac{\epsilon_p^2}{\epsilon_R^3} \quad (16)$$

$$\simeq 1 \times 10^{50} \text{ erg} \left(\frac{E_{\text{SN}}}{10^{51} \text{ erg}} \right) \left(\frac{\epsilon_p}{3} \right)^2 \left(\frac{\epsilon_R}{3} \right)^{-3}.$$

Assuming all CCSNe occur near the cluster center within the retained cluster gas around $t_{\text{age}} = 4-6 \text{ Myr}$, the total CCSN driving energy rate is

$$\left(\frac{dE}{dt} \right)_{\text{SN}} = \Gamma_{\text{SN}} K_{\text{SN}} M_{\star}$$

$$\simeq 1 \times 10^{40} \text{ erg s}^{-1} \left(\frac{\Gamma_{\text{SN}}}{5 \times 10^{-10} \text{ yr}^{-1} M_{\odot}^{-1}} \right) \left(\frac{K_{\text{SN}}}{10^{50} \text{ erg}} \right)$$

$$\times \left(\frac{M_{\star}}{6 \times 10^6 M_{\odot}} \right) \frac{1}{\mu_{300}}. \quad (17)$$

Despite much complexity in estimating CCSNe kinetic feedback in the radiative regime and with possibly inhomogeneous surrounding medium (Cowie et al. 1981), the order-of-magnitude agreement between Eq. (17) and Eq. (8) following simple estimations suggests that turbulence driving by CCSNe is at least plausible, provided that the cloud size R_g is not much larger than a fraction of pc and the turbulence velocity does not exceed $u = 100 \text{ km s}^{-1}$.

We note that having $\epsilon_R = 2-5$ puts $R_{\text{SN}} = 0.04-0.1 \text{ pc}$ for the fiducial values of E_{SN} and n_V , well within the size of the retained cluster gas $R_{\text{SN}} < R_g$. This is compatible with our physical picture here that CCSNe fail to remove the retained cluster gas, hence the efficient retention of their metal yield. SN remnant completely dissipates in the surrounding turbulent gas at the time $t_{\text{SN}} = \epsilon_t t_{\text{PDS}}$, where ϵ_t can be estimated

$$\epsilon_t \simeq 300 \left(\frac{u}{50 \text{ km s}^{-1}} \right)^{-\frac{10}{7}} \left(\frac{E_{\text{SN}}}{10^{51} \text{ erg}} \right)^{\frac{5}{49}}$$

$$\times \left(\frac{n_V}{10^{6.5} \text{ cm}^{-3}} \right)^{\frac{10}{49}} \xi_m^{-\frac{15}{49}}. \quad (18)$$

For our fiducial model parameters, the lifetime of each SN remnant is on the order of $t_{\text{SN}} \sim 10^3 \text{ yr}$ and is comparable to the inverse frequency of CCSN occurrence $1/(\Gamma_{\text{SN}} M_{\star})$. If CCSNe occur too frequently compared

to the remnant lifetime, complication can arise due to clustered feedback from multiple SNe, which should enhance SN momentum feedback (Gentry et al. 2019).

6.6. Effect of HI Column

Our picture of HII bubbles embedded in condensed, self-shielding cluster gas requires that emission lines traverse a large HI column before they leave the cluster gas. Intriguing, our emission line fitting favors a y value close to zero, which means we are mostly seeing emission line photons propagating through the self-shielded HI column rather than directly from the irradiated faces. According to `Cloudy`, we find this optical depth effect significantly decrease H Balmer lines for $y = 0$ but does not impact the metal (semi-)forbidden lines.

Ferland & Netzer (1979) studied line trapping of H Lyman and Balmer photons in an ionization-bounded HII region. In particular, trapped Ly α photons excite an $n = 2$ population which can provide a substantial resonant scattering optical depth to H Balmer photons, particularly in the absence of internal dust. As Grandi (1980) explains (also see Hamann (2012)), the trapped H α photons can convert to Ly β photons, which can pump the abundant O I ions in the neutral zone. H α can thus be lost when there is a substantial line optical depth to H Balmer photons.

Interestingly, we see a significant detection of O I λ 1641 (the line center is inconsistent with He II λ 1640), which is a fluorescent signature of Ly β pumping of O I. We refrain from quantitatively comparing the O I λ 1641 detection to `Cloudy` predictions, as the line trapping effect is sensitive to the column density, kinematics of the neutral gas behind the ionization front, and internal grain abundance.

This provides a promising explanation, which is perhaps more important than merely the elevated O and He abundances, for the surprising weakness of H Balmer lines as first pointed out by Vanzella et al. (2020b). We take this strong preference in data for an optical depth effect from a H I column as one more supporting evidence for our physical model for Godzilla’s nebular emission.

6.7. Ly α -pumped Fe III Fluorescence

Vanzella et al. (2020b) discovered remarkably bright fluorescent emission lines of Fe III from Godzilla, which are shown to result from Ly α excitation of a nearby Fe III λ 1214 transition (Johansson et al. 2000). To our knowledge, the only detailed report of this exact Fe III fluorescence process came from the Weigelt Blobs in η Car’s inner ejecta (Zethson et al. 2012), which are known to be heavily-CNO-processed material expelled

by η Car. Similar to what we have found for Godzilla’s nebula, the fluorescent Weigelt Blobs host dense ionized gas $n_e \sim 10^{(7-8)} \text{ cm}^{-3}$ (Hamann 2012) and exhibit large enhancement in N and He abundances (Verner et al. 2005), and shows fluorescent O I lines by Ly β pumping (Hamann 2012). Godzilla’s nebula gas appears to physically and chemically resemble the Weigelt Blobs, but is excited by a much brighter radiation source. This similarity perhaps explains why both are conducive to Ly α -pumped Bowen fluorescence.

Given the large $\sim 270 \text{ km s}^{-1}$ frequency de-tuning between H Ly α and the excited Fe III λ 1214 line, a strong and broad Ly α line has to form within the nebula. This requires a geometry in which Ly α photons are spatially trapped by repeated resonant scattering after they are produced from recombination. This also requires a dust-free condition so that the Ly α photons are not internally destroyed. In the case of Godzilla, ionization-bounded hot bubbles embedded in the cluster gas, which we postulate as the formation sites of the nebular emission lines, may provide the right geometry as the surrounding self-shielded component of the cluster gas is optically thick to Ly α photons. The cluster gas is also required to be dust-free, which appears consistent with non-detection of significant reddening of Godzilla’s FUV continuum. We therefore suggest, at least qualitatively, that our physical picture for Godzilla’s nebula may explain the observed Ly α -pumped Fe III fluorescence. We plan to investigate this in more details in a future publication.

6.8. Removal of Dust Grains

Our inferred relatively low $E(B - V) < 0.08$ implies that the overall nebula environment of Godzilla is not extremely dusty and is largely transparent to FUV. A grain-free condition is also required in the active zones to allow for H Lyman-series pumping and fluorescence.

As our photoionization modeling implies, direct stellar irradiation, dominated by FUV in energy, may be intense enough to vaporize dust grains. For the high radiation intensity, we neglect the effects of time-dependent temperature spikes for small grains, and only consider an equilibrium-state grain temperature T_d , which can be found by balancing the rate of FUV heating and the rate of cooling by thermal re-radiation at infrared wavelengths (Draine 2011a):

$$4\pi a^2 \langle Q \rangle_{T_d} \sigma_{\text{SB}} T_d^4 = \pi a^2 \langle Q \rangle_{\text{UV}} F_{\text{UV}}. \quad (19)$$

Here $\langle Q \rangle_{T_d}$ the absorption efficiency averaged over a Planck spectrum of temperature T_d , and $\langle Q \rangle_{\text{UV}}$ is the absorption efficiency averaged over the incident radiation, whose flux is dominated by UV photons, and σ_{SB} is the Stefan-Boltzmann constant.

The precise values of $\langle Q \rangle_{T_d}$ and $\langle Q \rangle_{UV}$ depend on grain size, grain composition, and the spectral shape of the incident star light, and are not always monotonic. For FUV photons $\langle Q \rangle_{UV} \simeq 1$. According to Figure 24.3 of [Draine \(2011a\)](#), we conservatively estimate:

$$\langle Q \rangle_{T_d} < 0.5 \left(\frac{a}{\mu\text{m}} \right), \quad (20)$$

in the temperature range $100 < T_d/\text{K} < 1000$, for sufficiently large grains $a > 0.01 \mu\text{m}$, and for both silicate and carbonaceous grains. These conservative limit leads to

$$\begin{aligned} T_d &> \left(\frac{(\mu\text{m}/a)}{0.5} \frac{\chi \Phi(\text{H}^0)}{4 \sigma_{\text{SB}}} \langle h\nu \rangle_{\text{ion}} \right)^{\frac{1}{4}} \\ &= 1200 \text{ K} \left(\frac{a}{0.01 \mu\text{m}} \right)^{-\frac{1}{4}} \\ &\times \left(\frac{\chi}{10} \right)^{\frac{1}{4}} \left(\frac{\Phi(\text{H}^0)}{10^{15.9} \text{ s}^{-1} \text{ cm}^{-2}} \right)^{\frac{1}{4}} \left(\frac{\langle h\nu \rangle_{\text{ion}}}{20 \text{ eV}} \right)^{\frac{1}{4}}. \end{aligned} \quad (21)$$

Here we have introduced the dimensionless χ , the ratio between the FUV flux and the ionizing flux. The lower bound is $T_d > 680 \text{ K}$ for $a = 0.1 \mu\text{m}$ and $T_d > 380 \text{ K}$ for $a = 1 \mu\text{m}$. Given the sublimation temperature $\sim 1200 \text{ K}$ for silicates and $\sim 1800 \text{ K}$ for carbonaceous grains, small silicates grains with $a \lesssim 0.01 \mu\text{m}$ could have been all evaporated by radiation, but large silicate grains or carbonaceous grains can likely survive.

For the geometry of embedded HII bubbles (Section 6.4.3), small silicate grains $a \lesssim 0.01 \mu\text{m}$ should be vaporized by individual O stars in the HII bubble vicinity, but it is unclear if the global FUV background throughout the retained gas cloud is intense enough to vaporize the other grains. Assuming that a fraction x_{FUV} of the FUV sources are enclosed within radius R_g , the mean FUV irradiation is a fraction $\simeq 0.16 (x_{\text{FUV}}/0.1) (R_g/0.3 \text{ pc})$ of the FUV irradiation in individual HII bubbles.

It may be that over time radiation pressure pushes all surviving grains out of the gas cloud. For grain collision with hydrogen atoms in an HI gas, [Draine & Salpeter \(1979\)](#) introduced the function

$$G(s) = \frac{8s}{3\sqrt{\pi}} \left(1 + \frac{9\pi}{64} s^2 \right)^{1/2}. \quad (22)$$

Here $s = v_d/\sqrt{2k_B T/m_p}$, where v_d is the grain drift velocity relative to the gas and T is the gas temperature. When the drift velocity is supersonic $s \gg 1$, $G(s) = s^2$.

Following [Draine \(2011b\)](#), we find a drift velocity

$$\begin{aligned} v_d &= 28 \text{ km s}^{-1} \left(\frac{\chi}{10} \right)^{\frac{1}{2}} \left(\frac{\Phi(\text{H}^0)}{10^{15.1} \text{ s}^{-1} \text{ cm}^{-2}} \right)^{\frac{1}{2}} \left(\frac{\langle h\nu \rangle_{\text{ion}}}{20 \text{ eV}} \right)^{\frac{1}{2}} \\ &\times \left(\frac{\langle Q_{\text{pr}} \rangle}{1.5} \right)^{\frac{1}{2}} \left(\frac{n_V}{10^{6.5} \text{ cm}^{-3}} \right)^{-\frac{1}{2}}, \end{aligned} \quad (23)$$

where $\langle Q_{\text{pr}} \rangle$ is the wavelength-averaged absorption efficiency. This is not small compared to the turbulence velocity u , so let us assume that turbulence motion does not significantly prohibit grain ejection. After a short time $R_g/v_d \approx 10^4 \text{ yr} (R_g/0.3 \text{ pc})/(v_d/30 \text{ km s}^{-1})$, FUV radiation should eject all grains out of the retained dense gas if they have survived sublimation.

In this process, dust grains drift relative to the gas at terminal speeds and exert an outward force on the gas as well. However, gravity of the cluster gas and the stars it encloses is strong enough to prevent gas from being ejected together with the dust grains. Indeed, the characteristic inward pressure due to gravity can be crudely estimated as

$$\begin{aligned} P_{\text{grav}} &\gtrsim \frac{G M_g^2}{R_g^4} \\ &\simeq 3 \times 10^{13} \text{ K cm}^{-3} \left(\frac{M_g}{10^5 M_\odot} \right)^2 \left(\frac{R_g}{0.3 \text{ pc}} \right)^{-4}. \end{aligned} \quad (24)$$

In comparison, the typical outward pressure from UV radiation transferred through the grain-gas coupling is significantly smaller

$$P_{\text{UV}} \simeq 10^{11} \text{ K cm}^{-3} \left(\frac{\Phi(\text{H}^0)}{10^{15.1} \text{ s}^{-1} \text{ cm}^{-2}} \right) \left(\frac{\langle h\nu \rangle_{\text{ion}}}{20 \text{ eV}} \right) \left(\frac{\chi}{10} \right). \quad (25)$$

6.9. Godzilla and Multiple Stellar Populations

The high mass and compactness of Godzilla make it a likely candidate for an analog progenitor of globular clusters ([Kruijssen 2014](#)), which ubiquitously host multiple stellar populations of distinct light element abundances (see [Bastian & Lardo \(2018\)](#) for a review). The dense nebula gas of Godzilla likely has accumulated inside the cluster, even at an age $t_{\text{age}} = 4\text{--}6 \text{ Myr}$ when the most massive stars have already started CC-SNe. While the standard expectation is that CCSNe will quickly clear out any cluster gas (e.g., [Calura et al. 2015](#); [D'Ercole et al. 2010](#)), the successful retention of stellar ejecta in Godzilla, if confirmed, will corroborate theoretical predictions that in dense star clusters feedback sometimes fails in doing this job (e.g., [Krause et al. 2013](#); [Tenorio-Tagle et al. 2016](#)), leaving behind a gas reservoir conducive to forming new generation of stars.

However, it does not seem likely to us that this particular dense nebula gas we are witnessing in Godzilla will birth the typical second generation (2P) stars. Assuming that CCSNe fail to expel the cluster gas, as appears to be the case in Godzilla, the strong turbulence driven by CCSNe feedback is expected to prohibit gravitational collapse (Hayward & Hopkins 2017), disfavoring formation of 2P stars after CCSNe onset. While some propose that this problem can be circumvented in the first 5–10 Myr of the cluster evolution by delaying the onset of CCSNe (e.g., Renzini et al. 2022), our inferred cluster age suggests that the delay of CCSNe onset may either be at most 1–2 Myr or does not happen at SMC-like stellar metallicities. Even if star formation still proves possible after CCSN onset, the observed simultaneous N and O enrichment is not compatible with the abundance pattern of the typical 2P stars, as they typically show N enhancement but no enhancement in α -elements. Should Godzilla be a true globular cluster progenitor, 2P star formation must have already occurred prior to the onset of CCSNe.

The observed enhancements in N/O and He/H should be primarily driven by wind ejecta (via comparison to MT12, see Figure 11). While our inferred N/O is broadly consistent with the 2P stars in globulars (Fig. 10), the inferred He/H value is likely too high. The He abundance in globulars typically has a small spread $\Delta Y \lesssim 0.1$, implying less than unity enhancement in the He/H ratio. By contrast, we infer a factor of ~ 2 –4 enhancement of He/H in Godzilla. Intriguingly, in some of the more special globular clusters such as ω Centauri, He/H differs by as much as a factor of two between multiple populations (Dupree & Avrett 2013), although it is unclear whether Godzilla could be a progenitor of such unique GCs. It is possible that the observed dense nebular gas is unrelated to 2P star formation, and the typical 2P star formation occurs even earlier, prior to the onset of He-rich winds from evolved massive stars. The models of MT12 find this onset at ~ 2.5 Myr, at which point CNO-processed material is ejected and enriches the surrounding with N and He. However, we note that there are likely earlier sources unaccounted for in the MT12 models that produce ejecta rich in N but not in He, such as Very Massive Stars (Vink 2023) or supermassive stars (Charbonnel et al. 2023). These sources would allow for similar N/O while significantly reduced (but still mildly enhanced) He/H to match what is observed in the majority of the GCs.

7. CONCLUSIONS

High lensing magnifications have offered a unique view of the impressive star formation activities on parsec

scales in the Cosmic Noon galaxy Sunburst. Apart from the 12-imaged Lyman-continuum-leaking super star cluster that has been previously studied, in this work we study Godzilla, which is seemingly a more perplexing source. We suggest that Godzilla is a young super star cluster with its core enshrouded with dense massive star ejecta photo-excited by stellar ionizing radiation. We have combined HST filter photometry and nebular emission line measurements from VLT/MUSE and X-shooter spectroscopy to model the star cluster and the associated nebula.

We find a cluster age 4–6 Myr and a likely stellar metallicity $Z = 0.25 Z_{\odot}$ for Godzilla. For a standard stellar IMF and depending on the total and tangential magnification factors μ and μ_t , we find a large cluster stellar mass $M_{\star} = 6 \times 10^6 M_{\odot} (300/\mu)$, and a PSF-based size constraint for its FUV-bright component, $R_{\text{FUV}} \lesssim 4 \text{ pc} (150/\mu_t)$. The high compactness should place Godzilla in a regime where rapid radiative cooling renders stellar wind and CCSNe material trapped in the cluster potential regardless of the initial ejecta speed. Indeed, despite the inferred SMC-like stellar metallicity, we found evidence for gas-phase He (He/H = $0.27^{+0.09}_{-0.10}$) and N ($\log \text{N/O} = -0.31^{+0.08}_{-0.08}$) enrichment indicative of massive star winds, as well as gas-phase O enhancement ($12 + \log \text{O/H} = 8.75^{+0.19}_{-0.25}$) indicative of CCSNe not long after onset. We also find sub-solar C/O, Ne/O and Si/O values in the nebula, which may have implications for CCSN light element yields for progenitor ZAMS masses greater than $40 M_{\odot}$.

Through a comparison to models of star cluster ejecta from MT12, we confirm that the inferred gas-phase abundances are consistent with complete retention of stellar winds and CCSN ejecta up to a cluster age around 4–6 Myr (Figure 11 and Figure 12), which also implies that stars more massive than $m_{\text{ZAMS}} = 40 M_{\odot}$ have successfully exploded and enriched the intracluster medium. We note that our inferred $\log \text{Ne/O} = -1.13^{+0.16}_{-0.13}$ is lower than the model prediction of MT12 and is interestingly lower than the solar value. While a large sample of less extreme star-forming regions show a solar Ne/O value independent of metallicity, Godzilla appears young enough that only stars more massive than about $40 M_{\odot}$ have reached the end of their lives. We therefore posit that the low Ne/O may be related to the CCSN yields of such massive progenitors, with speculations on photodisintegration of Ne to O through explosive nucleosynthesis and collapse of Ne-Mg-O shell into the remnant.

The nebula of Godzilla is remarkably dense $n_e \sim 10^{7-8} \text{ cm}^{-3}$, which indicates an extremely high intracluster pressure $P \sim 10^{11-12} \text{ K cm}^{-3}$. We suggest that the

high pressure is provided by supersonic turbulence in stellar ejecta that is accumulated in the cluster’s gravitational potential due to runaway radiative cooling, which is perhaps only a fraction of a parsec across (Section 6.4). The retained stellar ejecta is dense enough to self-shield against ionizing photons, is likely dust-free, and stays warm by UV heating. Through simple analytic analysis of CCSN kinetic feedback within a dense medium, we find that CCSNe after an age ~ 3 Myr, is possibly capable of maintaining this turbulence, but probably have failed to evacuate this enshrouding dense gas out of the cluster (Section 6.5). We theorize that nebular emission lines originate from many ionization-bounded hot bubbles that are blown either by massive star winds or by past CCSNe (see Figure 2). We have argued that such unusual geometry with a significant HI column along the line of sight may explain the weakness of H Balmer lines (Section 6.6) and the observed Ly α -pumped Fe fluorescent emission (Section 6.7).

Godzilla may be an analog of globular cluster progenitor at SMC-like metallicity. It is interesting to ponder whether the observed retained cluster gas would birth a 2P stellar population. However, the enhanced gas-phase O/H is not consistent with the typical abundance pattern of 2P stars. The gas-phase He/H elevation is consistent with pollution by evolved star winds, but is likely excessive compared to the typical He abundance variations seen in GCs. Altogether this implies that, should Godzilla be a true GC progenitor and host mul-

tipale stellar populations, the 2P stars probably have already formed, prior to the onset of evolved star winds and CCSNe which would dump excessive He and O respectively. This appears to align with very massive main sequence stars or supermassive stars as the polluters for multiple stellar population formation. Finding more objects similar to Godzilla will further shed light on these intriguing questions.

ACKNOWLEDGMENTS

Some of the data used in this paper were obtained from the Mikulski Archive for Space Telescopes (MAST) at the Space Telescope Science Institute. The specific observations analyzed can be accessed via this DOI.

We are foremost grateful to Christopher McKee for the countless inspiring discussions we had with him throughout the course of this work. We would like to also thank Luca Boccioli, Sanjana Curtis, Neal Dalal, Michael Fall, Xiao Fang, Brenda Frye, Mike Grudić, Alexander Ji, Chiaki Kobayashi, Wenbin Lu, Raffaella Margutti, Christopher Matzner, Shyam Menon, and Benny Tsang for the very valuable discussions and comments.

MP acknowledges funding support through the NSF Graduate Research Fellowship grant No. DGE 1752814, and acknowledges the support of System76 for providing computer equipment. L.D. acknowledges research grant support from the Alfred P. Sloan Foundation (Award Number FG-2021-16495), and support of Frank and Karen Dabby STEM Fund in the Society of Hellman Fellows.

REFERENCES

- Amorín, R., Fontana, A., Pérez-Montero, E., et al. 2017, *Nature Astronomy*, 1, 0052, doi: [10.1038/s41550-017-0052](https://doi.org/10.1038/s41550-017-0052)
- Arellano-Córdova, K. Z., Esteban, C., García-Rojas, J., & Méndez-Delgado, J. E. 2020, *MNRAS*, 496, 1051, doi: [10.1093/mnras/staa1523](https://doi.org/10.1093/mnras/staa1523)
- Arellano-Córdova, K. Z., Berg, D. A., Chisholm, J., et al. 2022, *ApJL*, 940, L23, doi: [10.3847/2041-8213/ac9ab2](https://doi.org/10.3847/2041-8213/ac9ab2)
- Asplund, M., Amarsi, A. M., & Grevesse, N. 2021, *A&A*, 653, A141, doi: [10.1051/0004-6361/202140445](https://doi.org/10.1051/0004-6361/202140445)
- Bastian, N., & Lardo, C. 2018, *ARA&A*, 56, 83, doi: [10.1146/annurev-astro-081817-051839](https://doi.org/10.1146/annurev-astro-081817-051839)
- Bayliss, M. B., Rigby, J. R., Sharon, K., et al. 2014, *ApJ*, 790, 144, doi: [10.1088/0004-637X/790/2/144](https://doi.org/10.1088/0004-637X/790/2/144)
- Berg, D. A., Erb, D. K., Auger, M. W., Pettini, M., & Brammer, G. B. 2018, *ApJ*, 859, 164, doi: [10.3847/1538-4357/aab7fa](https://doi.org/10.3847/1538-4357/aab7fa)
- Berg, D. A., Erb, D. K., Henry, R. B. C., Skillman, E. D., & McQuinn, K. B. W. 2019, *ApJ*, 874, 93, doi: [10.3847/1538-4357/ab020a](https://doi.org/10.3847/1538-4357/ab020a)
- Berg, D. A., Skillman, E. D., Henry, R. B. C., Erb, D. K., & Carigi, L. 2016, *ApJ*, 827, 126, doi: [10.3847/0004-637X/827/2/126](https://doi.org/10.3847/0004-637X/827/2/126)
- Berg, D. A., James, B. L., King, T., et al. 2022, *ApJS*, 261, 31, doi: [10.3847/1538-4365/ac6c03](https://doi.org/10.3847/1538-4365/ac6c03)
- Beroiz, M., Cabral, J. B., & Sanchez, B. 2020, *Astronomy and Computing*, 32, 100384, doi: [10.1016/j.ascom.2020.100384](https://doi.org/10.1016/j.ascom.2020.100384)
- Boccioli, L., & Roberti, L. 2024, arXiv e-prints, arXiv:2403.12942. <https://arxiv.org/abs/2403.12942>
- Bressan, A., Marigo, P., Girardi, L., et al. 2012, *MNRAS*, 427, 127, doi: [10.1111/j.1365-2966.2012.21948.x](https://doi.org/10.1111/j.1365-2966.2012.21948.x)
- Buchner, J., Georgakakis, A., Nandra, K., et al. 2014, *A&A*, 564, A125, doi: [10.1051/0004-6361/201322971](https://doi.org/10.1051/0004-6361/201322971)

- Calura, F., Few, C. G., Romano, D., & D’Ercole, A. 2015, *ApJL*, 814, L14, doi: [10.1088/2041-8205/814/1/L14](https://doi.org/10.1088/2041-8205/814/1/L14)
- Cameron, A. J., Katz, H., Rey, M. P., & Saxena, A. 2023, arXiv e-prints, arXiv:2302.10142, doi: [10.48550/arXiv.2302.10142](https://doi.org/10.48550/arXiv.2302.10142)
- Cantó, J., Raga, A. C., & Rodríguez, L. F. 2000, *ApJ*, 536, 896, doi: [10.1086/308983](https://doi.org/10.1086/308983)
- Carretta, E., Gratton, R. G., Lucatello, S., Bragaglia, A., & Bonifacio, P. 2005, *A&A*, 433, 597, doi: [10.1051/0004-6361:20041892](https://doi.org/10.1051/0004-6361:20041892)
- Charbonnel, C., Schaerer, D., Prantzos, N., et al. 2023, arXiv e-prints, arXiv:2303.07955, doi: [10.48550/arXiv.2303.07955](https://doi.org/10.48550/arXiv.2303.07955)
- Chevalier, R. A. 1974, *ApJ*, 188, 501, doi: [10.1086/152740](https://doi.org/10.1086/152740)
- Chevalier, R. A., & Clegg, A. W. 1985, *Nature*, 317, 44, doi: [10.1038/317044a0](https://doi.org/10.1038/317044a0)
- Chisholm, J., Rigby, J. R., Bayliss, M., et al. 2019, *ApJ*, 882, 182, doi: [10.3847/1538-4357/ab3104](https://doi.org/10.3847/1538-4357/ab3104)
- Christensen, L., Laursen, P., Richard, J., et al. 2012, *MNRAS*, 427, 1973, doi: [10.1111/j.1365-2966.2012.22007.x](https://doi.org/10.1111/j.1365-2966.2012.22007.x)
- Cioffi, D. F., McKee, C. F., & Bertschinger, E. 1988, *ApJ*, 334, 252, doi: [10.1086/166834](https://doi.org/10.1086/166834)
- Cowie, L. L., McKee, C. F., & Ostriker, J. P. 1981, *ApJ*, 247, 908, doi: [10.1086/159100](https://doi.org/10.1086/159100)
- Cox, D. P. 1972, *ApJ*, 178, 159, doi: [10.1086/151775](https://doi.org/10.1086/151775)
- Crowther, P. A., Schnurr, O., Hirschi, R., et al. 2010, *MNRAS*, 408, 731, doi: [10.1111/j.1365-2966.2010.17167.x](https://doi.org/10.1111/j.1365-2966.2010.17167.x)
- Dahle, H., Aghanim, N., Guennou, L., et al. 2016, *A&A*, 590, L4, doi: [10.1051/0004-6361/201628297](https://doi.org/10.1051/0004-6361/201628297)
- Dai, L., Kaurov, A. A., Sharon, K., et al. 2020, *MNRAS*, 495, 3192, doi: [10.1093/mnras/staa1355](https://doi.org/10.1093/mnras/staa1355)
- Danehkar, A., Oey, M. S., & Gray, W. J. 2021, *ApJ*, 921, 91, doi: [10.3847/1538-4357/ac1a76](https://doi.org/10.3847/1538-4357/ac1a76)
- de Mink, S. E., Pols, O. R., Langer, N., & Izzard, R. G. 2009, *A&A*, 507, L1, doi: [10.1051/0004-6361/200913205](https://doi.org/10.1051/0004-6361/200913205)
- Decressin, T., Meynet, G., Charbonnel, C., Prantzos, N., & Ekström, S. 2007, *A&A*, 464, 1029, doi: [10.1051/0004-6361:20066013](https://doi.org/10.1051/0004-6361:20066013)
- D’Ercole, A., D’Antona, F., Ventura, P., Vesperini, E., & McMillan, S. L. W. 2010, *MNRAS*, 407, 854, doi: [10.1111/j.1365-2966.2010.16996.x](https://doi.org/10.1111/j.1365-2966.2010.16996.x)
- Diego, J. M., Pascale, M., Kavanagh, B. J., et al. 2022, *A&A*, 665, A134, doi: [10.1051/0004-6361/202243605](https://doi.org/10.1051/0004-6361/202243605)
- Diego, J. M., Sun, B., Yan, H., et al. 2023, *A&A*, 679, A31, doi: [10.1051/0004-6361/202347556](https://doi.org/10.1051/0004-6361/202347556)
- Dopita, M. A., Fischera, J., Sutherland, R. S., et al. 2006, *ApJS*, 167, 177, doi: [10.1086/508261](https://doi.org/10.1086/508261)
- Dors, O. L., J., Krabbe, A., Hägele, G. F., & Pérez-Montero, E. 2011, *MNRAS*, 415, 3616, doi: [10.1111/j.1365-2966.2011.18978.x](https://doi.org/10.1111/j.1365-2966.2011.18978.x)
- Draine, B. T. 2011a, *Physics of the Interstellar and Intergalactic Medium*
- . 2011b, *ApJ*, 732, 100, doi: [10.1088/0004-637X/732/2/100](https://doi.org/10.1088/0004-637X/732/2/100)
- Draine, B. T., & Salpeter, E. E. 1979, *ApJ*, 231, 77, doi: [10.1086/157165](https://doi.org/10.1086/157165)
- Dupree, A. K., & Avrett, E. H. 2013, *ApJL*, 773, L28, doi: [10.1088/2041-8205/773/2/L28](https://doi.org/10.1088/2041-8205/773/2/L28)
- Erb, D. K., Pettini, M., Shapley, A. E., et al. 2010, *ApJ*, 719, 1168, doi: [10.1088/0004-637X/719/2/1168](https://doi.org/10.1088/0004-637X/719/2/1168)
- Federrath, C., Klessen, R. S., Iapichino, L., & Beattie, J. R. 2021, *Nature Astronomy*, 5, 365, doi: [10.1038/s41550-020-01282-z](https://doi.org/10.1038/s41550-020-01282-z)
- Ferland, G., & Netzer, H. 1979, *ApJ*, 229, 274, doi: [10.1086/156952](https://doi.org/10.1086/156952)
- Ferland, G. J., Chatzikos, M., Guzmán, F., et al. 2017, *RMxAA*, 53, 385. <https://arxiv.org/abs/1705.10877>
- Feroz, F., Hobson, M. P., & Bridges, M. 2009, *MNRAS*, 398, 1601, doi: [10.1111/j.1365-2966.2009.14548.x](https://doi.org/10.1111/j.1365-2966.2009.14548.x)
- Fosbury, R. A. E., Villar-Martín, M., Humphrey, A., et al. 2003, *ApJ*, 596, 797, doi: [10.1086/378228](https://doi.org/10.1086/378228)
- Garnett, D. R., Skillman, E. D., Dufour, R. J., et al. 1995, *ApJ*, 443, 64, doi: [10.1086/175503](https://doi.org/10.1086/175503)
- Gentry, E. S., Krumholz, M. R., Madau, P., & Lupi, A. 2019, *MNRAS*, 483, 3647, doi: [10.1093/mnras/sty3319](https://doi.org/10.1093/mnras/sty3319)
- Gieles, M., Charbonnel, C., Krause, M. G. H., et al. 2018, *MNRAS*, 478, 2461, doi: [10.1093/mnras/sty1059](https://doi.org/10.1093/mnras/sty1059)
- Grandi, S. A. 1980, *ApJ*, 238, 10, doi: [10.1086/157952](https://doi.org/10.1086/157952)
- Gray, W. J., Oey, M. S., Silich, S., & Scannapieco, E. 2019, *ApJ*, 887, 161, doi: [10.3847/1538-4357/ab510d](https://doi.org/10.3847/1538-4357/ab510d)
- Grimmett, J. J., Heger, A., Karakas, A. I., & Müller, B. 2018, *MNRAS*, 479, 495, doi: [10.1093/mnras/sty1417](https://doi.org/10.1093/mnras/sty1417)
- Hamann, F. 2012, in *Astrophysics and Space Science Library*, Vol. 384, *Eta Carinae and the Supernova Impostors*, ed. K. Davidson & R. M. Humphreys, 95, doi: [10.1007/978-1-4614-2275-4_5](https://doi.org/10.1007/978-1-4614-2275-4_5)
- Hayward, C. C., & Hopkins, P. F. 2017, *MNRAS*, 465, 1682, doi: [10.1093/mnras/stw2888](https://doi.org/10.1093/mnras/stw2888)
- Heger, A., & Woosley, S. E. 2002, *ApJ*, 567, 532, doi: [10.1086/338487](https://doi.org/10.1086/338487)
- Hennebelle, P., & Chabrier, G. 2008, *ApJ*, 684, 395, doi: [10.1086/589916](https://doi.org/10.1086/589916)
- Henry, R. B. C., & Worthey, G. 1999, *PASP*, 111, 919, doi: [10.1086/316403](https://doi.org/10.1086/316403)
- Hopkins, P. F. 2012, *MNRAS*, 423, 2016, doi: [10.1111/j.1365-2966.2012.20730.x](https://doi.org/10.1111/j.1365-2966.2012.20730.x)

- James, B. L., Pettini, M., Christensen, L., et al. 2014, *MNRAS*, 440, 1794, doi: [10.1093/mnras/stu287](https://doi.org/10.1093/mnras/stu287)
- Jaskot, A. E., & Ravindranath, S. 2016, *ApJ*, 833, 136, doi: [10.3847/1538-4357/833/2/136](https://doi.org/10.3847/1538-4357/833/2/136)
- Ji, A. P., Curtis, S., Storm, N., et al. 2024, *ApJL*, 961, L41, doi: [10.3847/2041-8213/ad19c4](https://doi.org/10.3847/2041-8213/ad19c4)
- Johansson, S., Zethson, T., Hartman, H., et al. 2000, *A&A*, 361, 977
- Keenan, F. P., Feibelman, W. A., & Berrington, K. A. 1992, *ApJ*, 389, 443, doi: [10.1086/171220](https://doi.org/10.1086/171220)
- Kewley, L. J., & Dopita, M. A. 2002, *ApJS*, 142, 35, doi: [10.1086/341326](https://doi.org/10.1086/341326)
- Kewley, L. J., Nicholls, D. C., & Sutherland, R. S. 2019, *ARA&A*, 57, 511, doi: [10.1146/annurev-astro-081817-051832](https://doi.org/10.1146/annurev-astro-081817-051832)
- Kim, K. J., Bayliss, M. B., Rigby, J. R., et al. 2023, *ApJL*, 955, L17, doi: [10.3847/2041-8213/acf0c5](https://doi.org/10.3847/2041-8213/acf0c5)
- Kobulnicky, H. A., & Kewley, L. J. 2004, *ApJ*, 617, 240, doi: [10.1086/425299](https://doi.org/10.1086/425299)
- Krause, M., Charbonnel, C., Decressin, T., Meynet, G., & Prantzos, N. 2013, *A&A*, 552, A121, doi: [10.1051/0004-6361/201220694](https://doi.org/10.1051/0004-6361/201220694)
- Kroupa, P. 2001, *MNRAS*, 322, 231, doi: [10.1046/j.1365-8711.2001.04022.x](https://doi.org/10.1046/j.1365-8711.2001.04022.x)
- Krujissen, J. M. D. 2014, *Classical and Quantum Gravity*, 31, 244006, doi: [10.1088/0264-9381/31/24/244006](https://doi.org/10.1088/0264-9381/31/24/244006)
- Leitherer, C., Ekström, S., Meynet, G., et al. 2014, *ApJS*, 212, 14, doi: [10.1088/0067-0049/212/1/14](https://doi.org/10.1088/0067-0049/212/1/14)
- Limongi, M., & Chieffi, A. 2018, *ApJS*, 237, 13, doi: [10.3847/1538-4365/aacb24](https://doi.org/10.3847/1538-4365/aacb24)
- Lochhaas, C., & Thompson, T. A. 2017a, *MNRAS*, 470, 977, doi: [10.1093/mnras/stx1289](https://doi.org/10.1093/mnras/stx1289)
- . 2017b, *MNRAS*, 470, 977, doi: [10.1093/mnras/stx1289](https://doi.org/10.1093/mnras/stx1289)
- López-Sánchez, Á. R., Esteban, C., García-Rojas, J., Peimbert, M., & Rodríguez, M. 2007, *ApJ*, 656, 168, doi: [10.1086/510112](https://doi.org/10.1086/510112)
- Mackey, J. 2023, in *Winds of Stars and Exoplanets*, ed. A. A. Vidotto, L. Fossati, & J. S. Vink, Vol. 370, 205–216, doi: [10.1017/S1743921322004501](https://doi.org/10.1017/S1743921322004501)
- Mainali, R., Rigby, J. R., Chisholm, J., et al. 2022, *ApJ*, 940, 160, doi: [10.3847/1538-4357/ac9cd6](https://doi.org/10.3847/1538-4357/ac9cd6)
- Marques-Chaves, R., Schaerer, D., Kuruvanthodi, A., et al. 2024, *A&A*, 681, A30, doi: [10.1051/0004-6361/202347411](https://doi.org/10.1051/0004-6361/202347411)
- Martell, S. L., Duffau, S., Milone, A. P., et al. 2013, *Mem. Soc. Astron. Italiana*, 84, 42, doi: [10.48550/arXiv.1301.4741](https://doi.org/10.48550/arXiv.1301.4741)
- McKee, C. F., & Ostriker, J. P. 1977, *ApJ*, 218, 148, doi: [10.1086/155667](https://doi.org/10.1086/155667)
- Mestric, U., Vanzella, E., Upadhyaya, A., et al. 2023, arXiv e-prints, arXiv:2301.04672, <https://arxiv.org/abs/2301.04672>
- Meynet, G., Ekström, S., & Maeder, A. 2006, *A&A*, 447, 623, doi: [10.1051/0004-6361:20053070](https://doi.org/10.1051/0004-6361:20053070)
- Mingozzi, M., James, B. L., Berg, D. A., et al. 2024, *ApJ*, 962, 95, doi: [10.3847/1538-4357/ad1033](https://doi.org/10.3847/1538-4357/ad1033)
- Mollá, M., & Terlevich, R. 2012, *MNRAS*, 425, 1696, doi: [10.1111/j.1365-2966.2012.21607.x](https://doi.org/10.1111/j.1365-2966.2012.21607.x)
- Nicholls, D. C., Sutherland, R. S., Dopita, M. A., Kewley, L. J., & Groves, B. A. 2017, *MNRAS*, 466, 4403, doi: [10.1093/mnras/stw3235](https://doi.org/10.1093/mnras/stw3235)
- Ostriker, J. P., & McKee, C. F. 1988, *Reviews of Modern Physics*, 60, 1, doi: [10.1103/RevModPhys.60.1](https://doi.org/10.1103/RevModPhys.60.1)
- Padoan, P. 1995, *MNRAS*, 277, 377, doi: [10.1093/mnras/277.2.377](https://doi.org/10.1093/mnras/277.2.377)
- Padoan, P., Federrath, C., Chabrier, G., et al. 2014, in *Protostars and Planets VI*, ed. H. Beuther, R. S. Klessen, C. P. Dullemond, & T. Henning, 77–100, doi: [10.2458/azu_uapress.9780816531240-ch004](https://doi.org/10.2458/azu_uapress.9780816531240-ch004)
- Pang, X., Grebel, E. K., Allison, R. J., et al. 2013, *ApJ*, 764, 73, doi: [10.1088/0004-637X/764/1/73](https://doi.org/10.1088/0004-637X/764/1/73)
- Pascale, M., Dai, L., McKee, C. F., & Tsang, B. T. H. 2023, *ApJ*, 957, 77, doi: [10.3847/1538-4357/acf75c](https://doi.org/10.3847/1538-4357/acf75c)
- Pettini, M., Steidel, C. C., Adelberger, K. L., Dickinson, M., & Giavalisco, M. 2000, *ApJ*, 528, 96, doi: [10.1086/308176](https://doi.org/10.1086/308176)
- Pignataro, G. V., Bergamini, P., Meneghetti, M., et al. 2021, arXiv e-prints, arXiv:2106.10286, <https://arxiv.org/abs/2106.10286>
- Pilyugin, L. S., Grebel, E. K., & Mattsson, L. 2012, *MNRAS*, 424, 2316, doi: [10.1111/j.1365-2966.2012.21398.x](https://doi.org/10.1111/j.1365-2966.2012.21398.x)
- Planck Collaboration, Ade, P. A. R., Aghanim, N., et al. 2014, *A&A*, 571, A29, doi: [10.1051/0004-6361/201321523](https://doi.org/10.1051/0004-6361/201321523)
- Reddy, N. A., Kriek, M., Shapley, A. E., et al. 2015, *ApJ*, 806, 259, doi: [10.1088/0004-637X/806/2/259](https://doi.org/10.1088/0004-637X/806/2/259)
- Renzini, A., Marino, A. F., & Milone, A. P. 2022, *MNRAS*, 513, 2111, doi: [10.1093/mnras/stac973](https://doi.org/10.1093/mnras/stac973)
- Rigby, J. R., Bayliss, M. B., Chisholm, J., et al. 2018, *ApJ*, 853, 87, doi: [10.3847/1538-4357/aaa2fc](https://doi.org/10.3847/1538-4357/aaa2fc)
- Rivera-Thorsen, T. E., Dahle, H., Gronke, M., et al. 2017, *A&A*, 608, L4, doi: [10.1051/0004-6361/201732173](https://doi.org/10.1051/0004-6361/201732173)
- Rivera-Thorsen, T. E., Dahle, H., Chisholm, J., et al. 2019, *Science*, 366, 738, doi: [10.1126/science.aaw0978](https://doi.org/10.1126/science.aaw0978)
- Rivera-Thorsen, T. E., Chisholm, J., Welch, B., et al. 2024, arXiv e-prints, arXiv:2404.08884, doi: [10.48550/arXiv.2404.08884](https://doi.org/10.48550/arXiv.2404.08884)
- Rogers, N. S. J., Skillman, E. D., Pogge, R. W., et al. 2022, *ApJ*, 939, 44, doi: [10.3847/1538-4357/ac947d](https://doi.org/10.3847/1538-4357/ac947d)

- Roy, A., Krumholz, M. R., Dopita, M. A., et al. 2022, in *The Origin of Outflows in Evolved Stars*, ed. L. Decin, A. Zijlstra, & C. Gielen, Vol. 366, 33–38, doi: [10.1017/S1743921322000722](https://doi.org/10.1017/S1743921322000722)
- Russell, S. C., & Dopita, M. A. 1992, *ApJ*, 384, 508, doi: [10.1086/170893](https://doi.org/10.1086/170893)
- Scherer, K., Fichtner, H., Kleimann, J., et al. 2016, *A&A*, 586, A111, doi: [10.1051/0004-6361/201526137](https://doi.org/10.1051/0004-6361/201526137)
- Schlegel, D. J., Finkbeiner, D. P., & Davis, M. 1998, *ApJ*, 500, 525, doi: [10.1086/305772](https://doi.org/10.1086/305772)
- Sedov, L. I. 1959, *Similarity and Dimensional Methods in Mechanics*
- Senchyna, P., Plat, A., Stark, D. P., & Rudie, G. C. 2023, arXiv e-prints, arXiv:2303.04179, doi: [10.48550/arXiv.2303.04179](https://doi.org/10.48550/arXiv.2303.04179)
- Senchyna, P., Stark, D. P., Vidal-García, A., et al. 2017, *MNRAS*, 472, 2608, doi: [10.1093/mnras/stx2059](https://doi.org/10.1093/mnras/stx2059)
- Sersic, J. L. 1968, *Atlas de Galaxias Australes*
- Sharon, K., Mahler, G., Rivera-Thorsen, T. E., et al. 2022, arXiv e-prints, arXiv:2209.03417, <https://arxiv.org/abs/2209.03417>
- Silich, S., Bisnovatyi-Kogan, G., Tenorio-Tagle, G., & Martínez-González, S. 2011, *ApJ*, 743, 120, doi: [10.1088/0004-637X/743/2/120](https://doi.org/10.1088/0004-637X/743/2/120)
- Silich, S., Tenorio-Tagle, G., & Rodríguez-González, A. 2004, *ApJ*, 610, 226, doi: [10.1086/421702](https://doi.org/10.1086/421702)
- Stanway, E. R., Eldridge, J. J., & Becker, G. D. 2016, *MNRAS*, 456, 485, doi: [10.1093/mnras/stv2661](https://doi.org/10.1093/mnras/stv2661)
- Stark, D. P., Richard, J., Siana, B., et al. 2014, *MNRAS*, 445, 3200, doi: [10.1093/mnras/stu1618](https://doi.org/10.1093/mnras/stu1618)
- Steidel, C. C., Strom, A. L., Pettini, M., et al. 2016, *ApJ*, 826, 159, doi: [10.3847/0004-637X/826/2/159](https://doi.org/10.3847/0004-637X/826/2/159)
- Stephenson, M. G., Arellano-Córdova, K. Z., Berg, D. A., Mingozzi, M., & James, B. L. 2023, *Research Notes of the American Astronomical Society*, 7, 31, doi: [10.3847/2515-5172/acbc12](https://doi.org/10.3847/2515-5172/acbc12)
- Stetson, P. B. 1987, *PASP*, 99, 191, doi: [10.1086/131977](https://doi.org/10.1086/131977)
- Stolte, A., Grebel, E. K., Brandner, W., & Figer, D. F. 2002, *A&A*, 394, 459, doi: [10.1051/0004-6361:20021118](https://doi.org/10.1051/0004-6361:20021118)
- Sung, H., & Bessell, M. S. 2004, *AJ*, 127, 1014, doi: [10.1086/381297](https://doi.org/10.1086/381297)
- Taylor, G. 1950, *Proceedings of the Royal Society of London Series A*, 201, 159, doi: [10.1098/rspa.1950.0049](https://doi.org/10.1098/rspa.1950.0049)
- Tenorio-Tagle, G., Muñoz-Tuñón, C., Cassisi, S., & Silich, S. 2016, *ApJ*, 825, 118, doi: [10.3847/0004-637X/825/2/118](https://doi.org/10.3847/0004-637X/825/2/118)
- Titova, A., Korolkov, S., & Izmodenov, V. 2021, *Journal of Physics: Conference Series*, 2028, 012012, doi: [10.1088/1742-6596/2028/1/012012](https://doi.org/10.1088/1742-6596/2028/1/012012)
- Vanzella, E., De Barros, S., Cupani, G., et al. 2016, *ApJL*, 821, L27, doi: [10.3847/2041-8205/821/2/L27](https://doi.org/10.3847/2041-8205/821/2/L27)
- Vanzella, E., Caminha, G. B., Calura, F., et al. 2020a, *MNRAS*, 491, 1093, doi: [10.1093/mnras/stz2286](https://doi.org/10.1093/mnras/stz2286)
- Vanzella, E., Meneghetti, M., Pastorello, A., et al. 2020b, *MNRAS*, 499, L67, doi: [10.1093/mnrasl/slaa163](https://doi.org/10.1093/mnrasl/slaa163)
- Vanzella, E., Castellano, M., Bergamini, P., et al. 2022, *A&A*, 659, A2, doi: [10.1051/0004-6361/202141590](https://doi.org/10.1051/0004-6361/202141590)
- Verner, E., Bruhweiler, F., & Gull, T. 2005, *ApJ*, 624, 973, doi: [10.1086/429400](https://doi.org/10.1086/429400)
- Vink, J. S. 2023, *A&A*, 679, L9, doi: [10.1051/0004-6361/202347827](https://doi.org/10.1051/0004-6361/202347827)
- Willner, S. P., & Nelson-Patel, K. 2002, *ApJ*, 568, 679, doi: [10.1086/339032](https://doi.org/10.1086/339032)
- Woosley, S. E., Heger, A., & Weaver, T. A. 2002, *Reviews of Modern Physics*, 74, 1015, doi: [10.1103/RevModPhys.74.1015](https://doi.org/10.1103/RevModPhys.74.1015)
- Woosley, S. E., Langer, N., & Weaver, T. A. 1993, *ApJ*, 411, 823, doi: [10.1086/172886](https://doi.org/10.1086/172886)
- . 1995, *ApJ*, 448, 315, doi: [10.1086/175963](https://doi.org/10.1086/175963)
- Wünsch, R., Palouš, J., Tenorio-Tagle, G., & Ehlerová, S. 2017a, *ApJ*, 835, 60, doi: [10.3847/1538-4357/835/1/60](https://doi.org/10.3847/1538-4357/835/1/60)
- . 2017b, *ApJ*, 835, 60, doi: [10.3847/1538-4357/835/1/60](https://doi.org/10.3847/1538-4357/835/1/60)
- Wünsch, R., Silich, S., Palouš, J., Tenorio-Tagle, G., & Muñoz-Tuñón, C. 2011, *ApJ*, 740, 75, doi: [10.1088/0004-637X/740/2/75](https://doi.org/10.1088/0004-637X/740/2/75)
- Yeh, S. C. C., & Matzner, C. D. 2012, *ApJ*, 757, 108, doi: [10.1088/0004-637X/757/2/108](https://doi.org/10.1088/0004-637X/757/2/108)
- Zethson, T., Johansson, S., Hartman, H., & Gull, T. R. 2012, *A&A*, 540, A133, doi: [10.1051/0004-6361/201116696](https://doi.org/10.1051/0004-6361/201116696)